mater.scichina.com link.springer.com

Published online 18 January 2023 | https://doi.org/10.1007/s40843-022-2316-y
Sci China Mater 2023, 66(3): 839–858

Metal-organic layers: Preparation and applications

Huifeng Wang[1,2], Chao Zhang[1], Baoxia Dong[2], Dichang Zhong[1*] and Tongbu Lu[1*]

ABSTRACT Metal-organic layers (MOLs) have attracted considerable interest in materials science because of their unique characteristics. The past decade has witnessed the rapid development of MOLs in synthesis and applications. Here we present a review of the latest research advances on MOLs. First, we introduce the two preparation approaches for MOLs, namely, the top-down and bottom-up approaches. Then, we discuss the applications of MOLs in gas separation, catalysis, energy catalysis and conversion, and chemical sensors, which emphasize the performance-morphologies/structures relationship of MOLs. At the end of this review, we provide an outlook on the opportunities and challenges of MOLs in the future.

Keywords: metal-organic layers, MOF nanosheets, 2D materials, metal-organic frameworks

INTRODUCTION

Metal-organic frameworks (MOFs) made by bridging metal-containing nodes with organic ligands are a type of ordered porous material [1–3]. The first case of MOFs reported by Yaghi *et al.* [4] in 1995 sparked a frenzy in the research on MOFs. The past decade has witnessed the rapid development of such types of materials [5–9]. However, because of the limitation on material thickness, their applications in separation, catalysis, and biosensors are inevitably adversely affected [10–14]. The preparation of two-dimensional (2D) ultrathin MOF nanosheets (also called metal-organic layers (MOLs)) could be an alternative to further enhance or extend the functionalities of MOFs [15–19]. In MOLs, active centers are well exposed on the surface, which facilitates the interaction between vibrant centers and substrate molecules [20–25], thus, improving their applications in catalysis, gas separation, and sensing [26–34]. The MOLs are commonly prepared by the top-down or bottom-up method [35–40]. The top-down method uses physical or chemical means to exfoliate bulk MOFs into MOLs [41–53], whereas the bottom-up method synthesizes 2D MOLs by constraining the growth of MOLs in the third direction [50–64]. Both methods have been extensively used to prepare 2D ultrathin MOLs with sub-10 nm thicknesses in the past decade [65–67].

In 2008, Fjellvåg and coworkers [68] reported the first exfoliated MOF material prepared *via* ultrasonication. It marked the beginning of the use of the top-down approach to prepare 2D MOLs. In 2010, Kitagawa and coworkers [69] combined layer-by-layer (LBL) growth with the Langmuir-Blodgett (L-B) method to prepare (4-methoxyphenyl)porphyrin (TCPP)-based MOF nanofilm under mild conditions. It was a typical bottom-up method. In 2014, Yang and coworkers [70] developed a wet ball milling technique to exfoliate a layer-structured MOF of $Zn_2(bim)_4$ (bim = benzimidazole). In 2016, Zhu and coworkers [71] successfully obtained Cu-BHT (BHT = benzenehexathiol) nanosheets *via* the interfacial synthesis method. With this method, the flat interfaces formed by two heterogeneous phases can block the vertical overgrowth of the nanosheets, thus ensuring the growth of MOF in a limited 2D interface area, which promotes the formation of the MOLs. In 2018, Zhang and coworkers [36] first demonstrated an electrochemical exfoliation approach to produce MOLs. This approach can circumvent the utilization of surfactants, thus, boosting the active metal sites on the FeCo-MNS (MNS = MOF-74 nanosheets) surface interacting with the reactants. The exfoliated nanosheets exhibit excellent stability and improved catalytic activity. Recently, our group developed a ligand replacement strategy to prepare 2D MOLs from 3D MOFs [72]. The terminal capping ligands with stronger coordination capacity replace the pillar bridging ligands in 3D pillared-layer MOFs, adequately and efficiently yielding 2D MOLs on a large scale. The resulting hydrophobic MOLs exhibit good oil/water separation performance.

Although the studies on 2D materials have been summarized by several groups [15,17,22,23,25,73–75], those focused on the syntheses and applications of 2D MOLs have not been specifically and systematically reported. In this review, we thoroughly introduce and discuss the preparation and applications of the newly emerging 2D material, that is, MOLs. First, we summarize the two synthesis strategies for preparing 2D MOLs. Then, we discuss their applications in gas separation, catalysis, energy conversion, and sensing and emphasize the relationship between their functions and structures. Finally, we present the challenges and opportunities for MOL materials in the future.

PREPARATION

Two strategies, namely, top-down and bottom-up, are commonly employed to prepare 2D MOLs. The top-down method can be divided into physical and chemical exfoliation, corresponding to the precursors of 2D layered MOFs and 3D pillared MOFs, respectively [21]. The bottom-up method includes interfacial synthesis [71,76], surfactant-assisted synthesis [55,77], and template-assisted synthesis [78,79]. Both methods target the same goal, that is, to obtain 2D MOLs with desirable

[1] Institute for New Energy Materials & Low-Carbon Technologies, School of Materials Science and Engineering, Tianjin University of Technology, Tianjin 300384, China
[2] College of Chemistry and Chemical Engineering, Yangzhou University, Yangzhou 225002, China
[*] Corresponding authors (emails: zhong_dichang@hotmail.com (Zhong D); lutongbu@tjut.edu.cn (Lu T))

characteristics.

Top-down method

The top-down method for MOL preparation can be defined as disintegrating bulky MOFs into single-layer or multilayer MOF nanosheets [18], where the exfoliation of bulky MOFs is essential to obtain 2D MOLs, including physical and chemical approaches.

Physical exfoliation

Physical exfoliation is a conventional approach to obtain 2D MOLs from MOFs with layered structures [21,80–84]. In 2008, Fjellvåg and coworkers [68] performed MOF exfoliation experiments to produce MOLs. They determined that the solvent is an important factor affecting the exfoliating effect. Single-layer or two-layer MOLs of $Zn(C_{12}H_{14}O_4)$ were prepared in acetone and ethanol solvents with high polarity and small molecular size. Two years later, Zamora and coworkers [80] produced 2D MOLs from lustrous bulky $[Cu_2Br(IN)_2]_n$ (IN = isonicotinato), where ultrasound was employed to disrupt the interlayer π–π interaction. The atomic force microscopy (AFM) image showed dense flakes homogeneously distributed on the highly oriented pyrolitic graphite (HOPG) substrate. The observed height of 5.00 ± 0.15 Å is consistent with the thickness expected for a single layer. In 2011, Xu and coworkers [81] reported that MOF-2 could be exfoliated into MOLs by ultrasonication in acetone. The AFM images showed that the thickness of MOLs is in the range of 1.5–6.0 nm and the lateral dimension varies from 100 nm to 1 μm. Ultrasonication is a simple and effective approach to prepare MOL materials. However, obtaining surface-clean MOLs with uniform thickness by sonication is still a challenge.

The exfoliation of bulky MOFs only by ultrasonication may also destroy the in-plane structure of the resulting MOLs [85,86]. To address this problem, Yang and coworkers [70] combined ultrasonic treatment with the wet ball milling technique to exfoliate a layered MOF of $Zn_2(bim)_4$ (Fig. 1a). As the adjacent layers in $Zn_2(bim)_4$ are bound by van der Waals forces (Fig. 1b, c), the wet ball milling process at a low speed of 60 r min^{-1}, together with the ultrasonic exfoliation process in the mixture of propanol and methanol, could efficiently prepare $Zn_2(bim)_4$ MOLs. They also determined that small molecules like methanol could penetrate the layered $Zn_2(bim)_4$, and propanol could stabilize the resulting MOLs by attaching them to the surface of MOLs with hydrophobic aliphatic chains. The MOLs dispersed in solution exhibit the Tyndall effect (Fig. 1d). The thickness of the resulting MOLs is 1.12 nm (Fig. 1e, f). The case reveals the importance of solvents in bulky MOFs exfoliation. Three years later, Yang and coworkers [87] further prepared $Zn_2(bim)_3$ MOLs *via* the top-down method. The obtained $Zn_2(bim)_3$ MOLs have a thickness of 1.6 nm, corresponding to a structure with two layers.

Zhao and coworkers [88,89] developed a mild exfoliation method for obtaining 2D MOLs with perfect morphology, as the fragmentation of 2D MOLs will affect the subsequent fabrication of MOL membranes. A freeze-thaw method was developed for the mild exfoliation of MOFs to prepare MOLs. Based on MOF MAMS-1 with a 2D layered structure and excellent hydro-

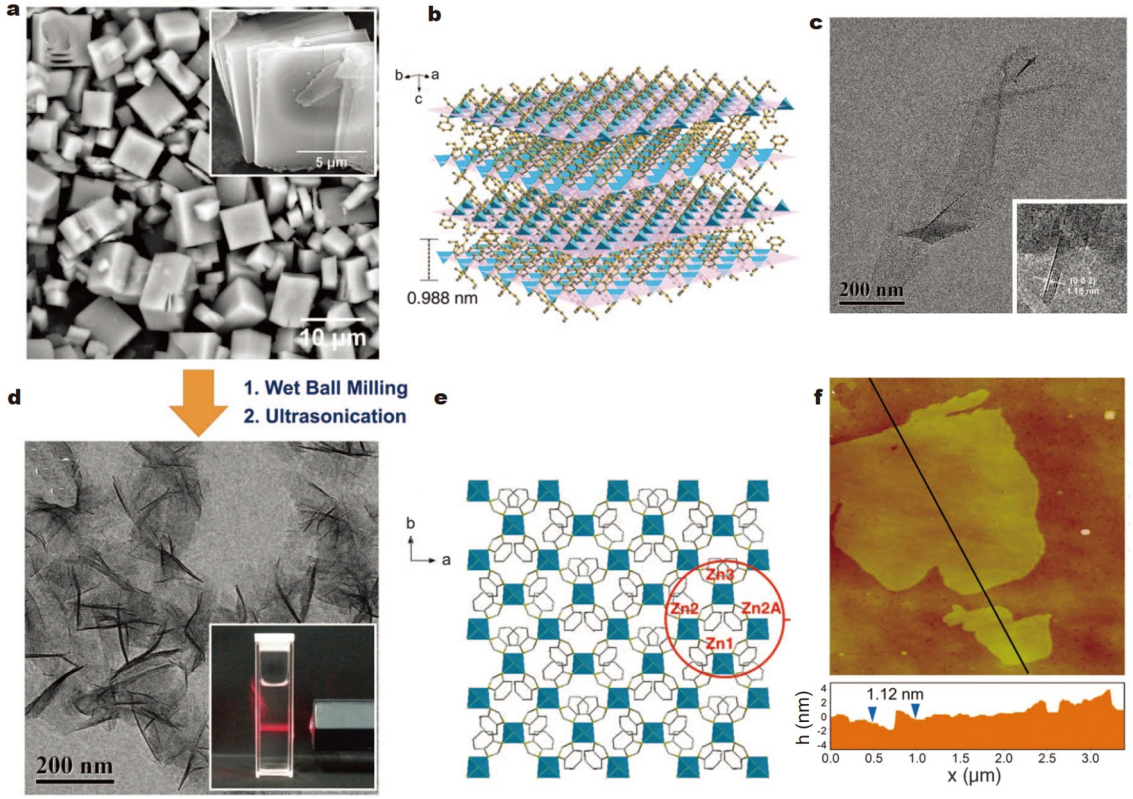

Figure 1 (a) Scanning electron microscopy (SEM) image of bulky $Zn_2(bim)_4$. (b) 3D supramolecular structure of the layered $Zn_2(bim)_4$. (c, d) Transmission electron microscopy (TEM) images, (e) 2D grid-like layer structure, and (f) AFM image of $Zn_2(bim)_4$ MOLs (supported on a silicon wafer). Reprinted with permission from Ref. [70], Copyright 2014, The American Association for the Advancement of Science.

thermal stability, the repeated freeze-thaw cycles could mildly exfoliate MAMS-1 bulky crystals into 2D MOLs [88]. During the exfoliation process, the bulky MAMS-1 was suspended in hexane, frozen in a liquid nitrogen bath (−196°C), and thawed in an 80°C water bath (Fig. 2a). The shear force induced by the change of the hexane volume during solid-liquid phase transition was applied to the suspended bulky MAMS-1, which led to the exfoliation of the bulky MAMS-1 into individual MOLs. The thickness of the MOLs is approximately 4 nm, corresponding to bilayered MAMS-1 structure (Fig. 2b). Aside from 2D layered MOFs, 3D MOFs can also be exfoliated into MOLs by physical exfoliation.

In 2017, Grey and coworkers [90] reported a 2D hafnium-based MOL, which was derived from the exfoliation of 3D hcp UiO-67 (a 3D hafnium-containing MOF) or 2D hxl UiO-67 (a 2D hafnium-containing MOF). The hcp UiO-67 and hxl UiO-67 could reversibly transform. Both 3D hcp UiO-67 and 2D hxl UiO-67 could be delaminated by grinding/sonication to obtain 2D MOLs with a thickness of 11 nm. Zhang and coworkers [91] also demonstrated that a 3D pillared-layer MOF could be transformed into 2D MOLs after multistep evolution. First, they found that the 3D pillared-layer MOF of $(H_3O)_2[Cd_4(dhbdc)_2(H_2dhbdc)(DMF)_4]\cdot H_2O$ (3D-Cd-MOF, H_4dhbdc = 2,3-dihydroxy-1,4-benzenedicarboxylic acid, DMF = *N*,*N*-dimethylformamide) can rapidly transform into a 2D MOF of $[Cd_4(dhbdc)_2(H_2O)_8]\cdot 2H_2O\cdot H_4dhbdc$ (2D-Cd-MOF) in H_2O. When the latter was further sonicated in H_2O, MOLs with the formula of $[Cd_2(dhbdc)(H_2O)_4]$ could be obtained. SEM revealed that the resulting MOLs have a thin slice morphology, TEM showed wrinkled or ruptured nanosheets, and AFM yielded a thickness of 1.0 nm.

The coordination bonds in the 3D pillared-layer structure have apparent anisotropy. Through the cooperation of host-guest interactions and ultrasonication, the structural transformation of controllable orientation can be realized, and monolayer MOLs can be prepared. In this way, Huang and coworkers [92] prepared ultrathin MOLs from a 3D pillared-layer Zn MOF. With the help of host-guest interactions and ultrasonication, the 3D Zn MOF was readily exfoliated into 2D single-layer MOL nanosheets, with a yield of approximately 94% and a thickness of approximately 0.9 nm.

The aforementioned cases indicate that physical exfoliation is an effective method to prepare surface-clean and highly crystalline 2D MOLs. However, this method also faces many challenges. For instance, the yield and productivity are usually too low, which limits practical applications. Moreover, stabilizing MOLs against restacking is rather challenging. Therefore, other methods need to be developed to solve these problems, despite an investigation that has shown that the solvent effect may improve yield and MOL stabilization [18].

Chemical exfoliation

As discussed previously, although the physical technique can effectively produce 2D MOLs, the preparation of MOLs with controllable thickness in high yield is still a challenge. To overcome this problem, the development of other approaches by which 2D uniform MOLs can be efficiently prepared on a large scale is needed. Aida and coworkers [93] reported a chemical approach to selectively delaminate layered MOFs into 2D MOLs [93]. In their work, they focused on a layer-structured Cu(II) MOF with a kagome topological network. When immersed in DMF or tetrahydrofuran (THF), this MOF expands rapidly like an accordion. Notably, when further immersed in a suitable solvent, State II and state III crystals were preferentially delaminated into bilayer and monolayer MOLs, respectively. More importantly, the crystal structures of three states (i.e., I–III) were successfully identified, clearly demonstrating the process of MOL formation. Lin and coworkers [40] developed photochemical tactics for the *in situ* exfoliation of 2D MOFs. They prepared two MOFs of M_2TCPE (M = Ni or Co, TCPE = 1,1,2,2-tetra(4-carboxylphenyl)ethylene). They determined that, in the photocatalytic process, both MOFs experienced *in situ* exfoliation to obtain MOLs and assumed the Tyndall effect. This is the first report of 2D MOLs obtained by photochemical *in situ* exfoliation. They recycled the catalytic experiments for five runs with the same reaction conditions and determined that, with the increase of the cycling times, the Tyndall effect of the solution after catalysis was significantly enhanced.

This finding indicates that the size of these MOFs gradually decreased to nanosheets, which was further confirmed by SEM and TEM measurements. The AFM image shows that the average thickness of MOLs is approximately 6.5 nm. Furthermore, Zhang and coworkers [94] demonstrated an electrochemical strategy to *in situ* delaminate 2D MOFs into ultrathin MOLs. They determined that, during the electrocatalytic procedure, the highly crystalline 2D MOFs $[Ln^{III}Ni^{II}_4L_2(H_2O)_8](ClO_4)_3\cdot nH_2O$ (Ln = Ce/La/Pr, n = 6/7) transformed into an amorphous phase (Fig. 3a). SEM and TEM measurements revealed that the 2D MOFs changed into wrinkled thin MOLs, which are approximately 4 nm thick (Fig. 3b).

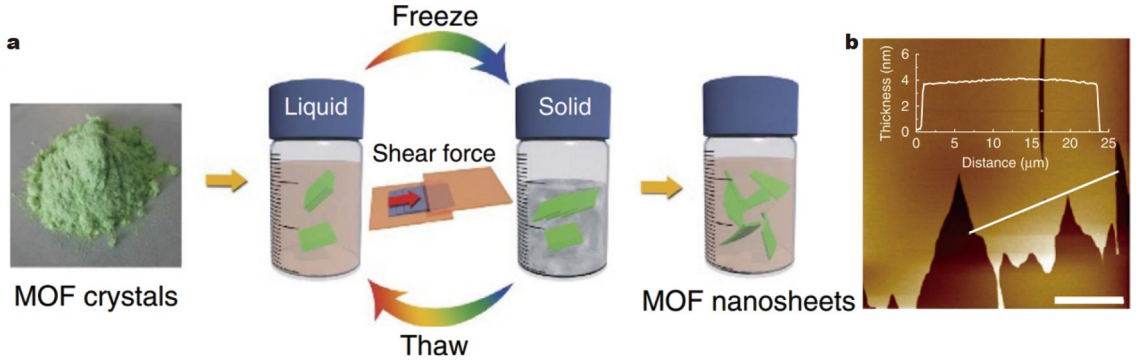

Figure 2 (a) Freeze-thaw exfoliation method to prepare MAMS-1 MOLs. (b) AFM image of MAMS-1 MOLs. Scale bar, 10 μm. Reprinted with permission from Ref. [88], Copyright 2017, Nature Publishing Group.

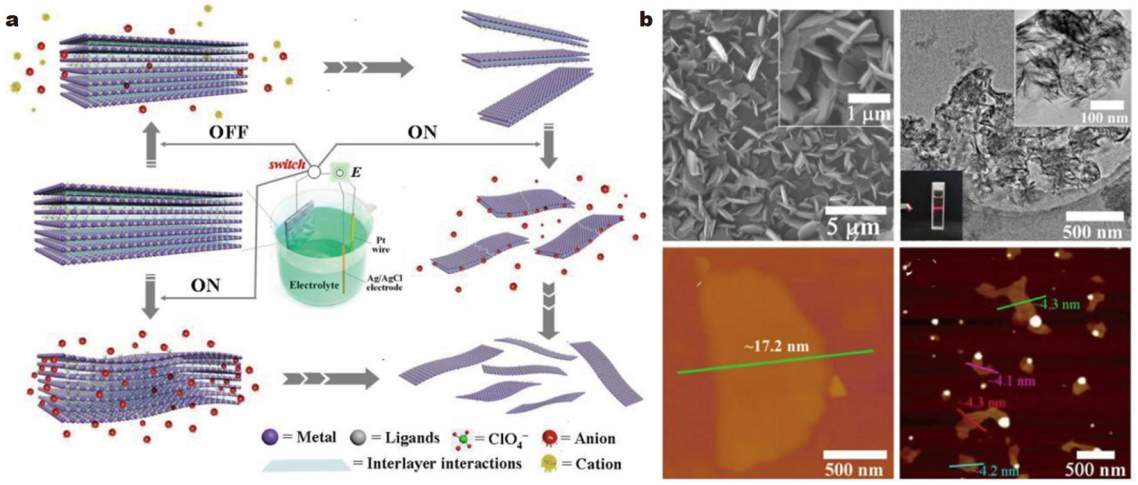

Figure 3 (a) Electrochemical strategy to exfoliate bulky 2D MOF into MOLs. (b) SEM, TEM, and AFM images of bulky MOFs. Reprinted with permission from Ref. [94], Copyright 2020, American Chemical Society.

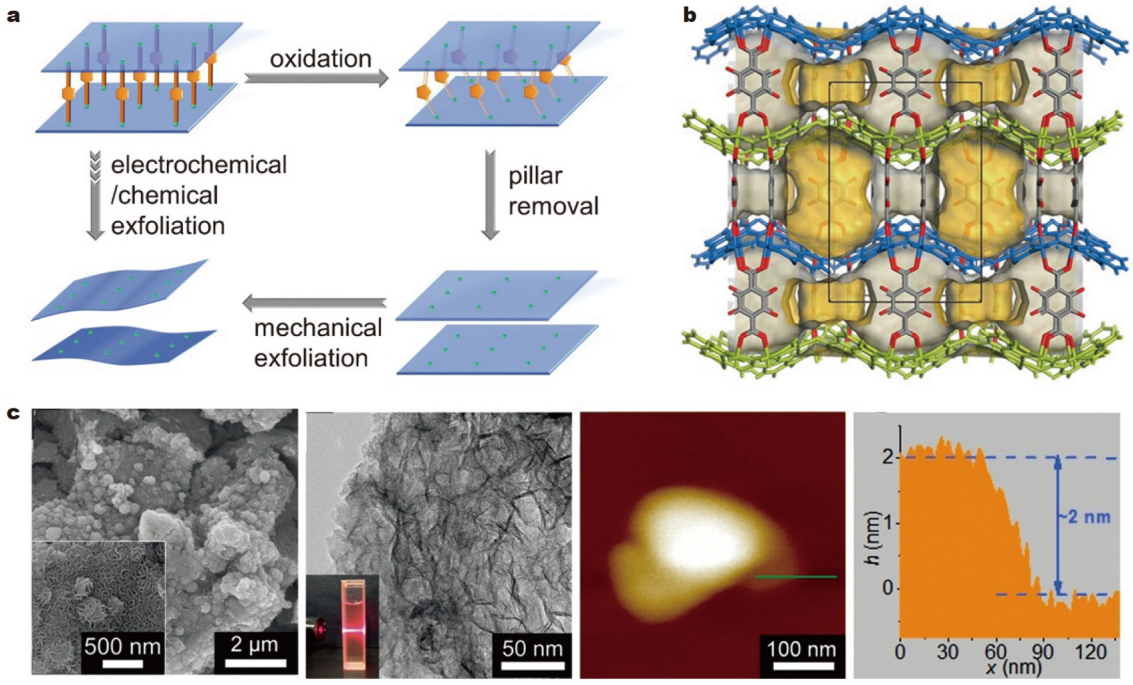

Figure 4 (a) Electrochemical exfoliation approach to prepare 2D MOLs from a 3D pillared-layer Co MOFs. (b) 3D pillared-layer Co MOF. (c) SEM, TEM, and AFM images of the resulting 2D Co MOLs. Reprinted with permission from Ref. [36], Copyright 2018, Wiley-VCH.

Aside from 2D layered MOFs, chemical exfoliation can also be used to delaminate 3D MOFs. In 2017, Zhou and coworkers [28] used a chemical exfoliation strategy to obtain MOLs from a constitutionally layered MOF. First, a porphyrinic MOF with a layered structure was intercalated with 4,4′-dipyridyl disulfide *via* coordination interactions. Second, the selective fracture of disulfide bonds resulted in the exfoliation of the embedded porous crystals and the formation of independent porous MOLs. This chemical exfoliation approach can achieve approximately 57% overall yield of 2D MOL product at room temperature.

The electrochemical exfoliation approach can also be used to exfoliate 3D MOFs to prepare 2D MOLs (Fig. 4a) [36]. Zhang and coworkers [36] designed a 3D pillared-layer Co MOF consisting of wavelike $[Co_6O(dhbdc)_2]^{2+}$ layer and 2,3-dihydroxy-1,4-benzene dicarboxylic acid(H_2dhbdc) pillar. The pillar is redox-active and can be oxidized and removed. As a result, after electrolysis, the 3D crystalline Co MOF is converted into amorphous 2D Co nanosheets. SEM and TEM show that the morphology of the MOLs is ultrathin and wrinkled (Fig. 4b), with approximately 2 nm thick (Fig. 4c). They further determined that 3D pillared-layer MOFs could be exfoliated into ultrathin MOLs in H_2O or $NH_3{\cdot}H_2O$ solution [95].

In 2019, we developed a ligand replacement strategy to adequately produce 2D MOLs from 3D pillared-layer MOFs [72]. The fundamental principle of this strategy is based on coordination equilibrium; that is, the organic ligands with stronger coordination affinity would substitute those with weaker coordination affinity to bond with metal ions. With this concept, we

synthesized two 3D pillared-layer MOFs with 4,4′-bipyridine (bpy) as the pillar ligand [96]. After being immersed in the methylated pyridine solution for a certain period, the interlayer bpy pillars were replaced with methylated pyridine capping ligands, and the adjacent layers were broken to form 2D MOLs. The formation process of the MOLs was monitored by SEM. Notably, the MOF flakes were exfoliated and became thin enough to curl up easily. Nearly all of the resulting MOLs have monolayer thickness. Using the same method, we further obtained Co MOLs from a 3D pillared-layer bulky Co MOF on a large scale (Fig. 5a) [97]. The mixed solution is orange at the beginning of exfoliation and gradually converted into a clear and transparent pink over time. After successful exfoliation, the Tyndall effect can be observed in the mixed solution. The AFM image shows that the micromorphology of the resulting Co MOLs is ultrathin (1.5 nm; Fig. 5b). The obtained Co MOLs could be used as a type of precursor to prepare a single Co site catalyst for photochemical CO_2 reduction to CO.

Bottom-up method

The critical point of the bottom-up method in MOL synthesis is to prevent the MOFs from growing in the vertical direction or the secondary growth of the resulting MOLs. This method usually includes interfacial synthesis, direct solvothermal synthesis, and template synthesis.

Interfacial synthesis

Interfacial synthesis has been widely used to grow MOLs. This method, utilizing the extended interfaces between two phases (such as liquid-liquid, liquid-gas, and liquid-solid), can prevent the vertical overgrowth of the nanosheets and ensure the growth of MOF in a limited interface area, which promotes the formation of MOLs. Using this method, Zhu and coworkers [71] synthesized Cu-BHT MOLs by reacting Cu(II) metal salts and BHT at the dichloromethane (CH_2Cl_2)-water interface. In the Ar environment, BHT was first dissolved in a CH_2Cl_2-filled bottle with Ar and then covered with H_2O to form a water-oil interface. The copper salt was dissolved in H_2O and slowly added to the aqueous phase using a syringe. Finally, the film formation could be observed intuitively at the interface. The formation of thin films can be visually observed at the methylene chloride-water interface. As the thickness increases, the formed film gradually becomes opaque. The SEM images showed that the top surface of the Cu-BHT MOL was flat and continuous without any folds or cracks. However, the growth direction of MOL was random, resulting in a rough bottom surface. AFM analysis also revealed the increased roughness of the bottom surface with the increase in the thickness of MOL. Meanwhile, the smoothness of the top surface remained unchanged (Fig. 6a–e). Notably, the initial MOLs were flat. However, as the thickness of the MOLs increased, the interface-confining effect was weakened, resulting in coarse MOLs. Notably, the extent of this effect could be regulated by the length of the reaction time. Using the same water-CH_2Cl_2 interface, several other MOLs have also been fabricated [37,98–100]. Moreover, the interface of water-ethyl-acetate could be used to prepare Co-BHT and Co-THT (THT = 1,2,5,6,9,10-triphenylenehexathiol) MOLs [101,102].

Aside from the aforementioned immiscible liquid interface, the preparation of MOLs can also be achieved by adding a diffusion medium to a miscible solution. Typically, this strategy consists of three liquid layers, that is, gently adding an optimized transition layer between the bottom and top layers, which determines the diffusion rates of metal ions and ligands. Gascon and coworkers [76] favorably synthesized ultrathin Cu-BDC MOL (H_2BDC = 1,4-benzenedicarboxylic acid) through a three-layer liquid method. In their work, the DMF solution of H_2BDC was placed in a vial as the bottom layer, the mixture of DMF and CH_3CN was added as the transition layer, and the CH_3CN solution with $Cu(NO_3)_2$ was added as the top layer. The bottom layer contained a high-density solution of DMF that dissolved the organic ligands, the top layer contained a low-density CH_3CN solution that dissolved the metal ions, and the transition layer contained an equal amount of DMF and CH_3CN that served as a buffer area to slow down the diffusion rates of Cu^{2+} and BDC^{2-}. The gradual diffusion of Cu^{2+} cations and BDC^{2-} anions into the interstitial region yielded MOLs in a highly diluted medium. SEM and AFM revealed square lamellae with 0.5–4 μm lateral dimensions and 5–25 nm thicknesses. TEM confirmed the highly regular morphology of the as-obtained MOLs.

As an interfacial synthesis method, the L-B approach was also employed to synthesize ordered monolayer MOLs. In 2010, Kitagawa and coworkers [69] combined the LBL growth method with the L-B approach to prepare TCPP-based MOL films. First, dispensing a methanol/chloroform solution containing CoTCPP and pyridine onto an aqueous solution containing $CuCl_2$, a subphase of 2D CoTCPP-py-Cu sheets was formed at the interface. Then, the sheets were supported on a quartz substrate, and stacking was conducted through a continuous LBL growth process, including the intermediate rinsing and immersion steps, thereby obtaining the TCPP-based MOLs. The L-B method has also been used to synthesize other MOLs [37,101,103–106]. The

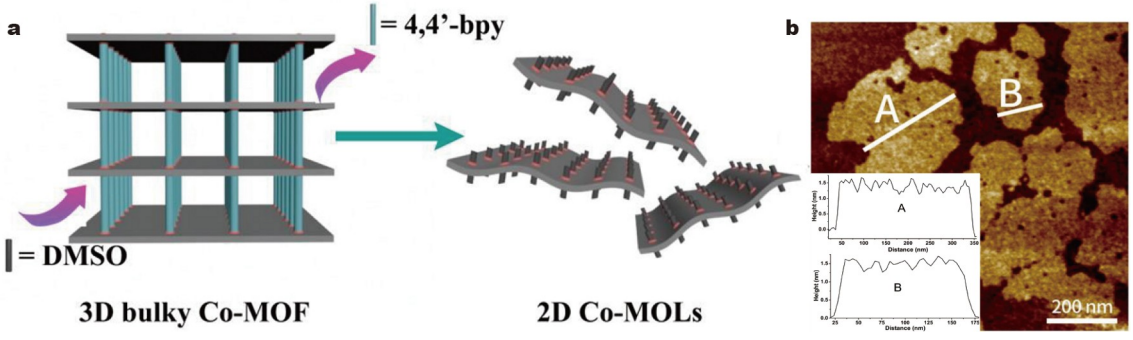

Figure 5 (a) Preparation process of 2D Co MOLs. (b) AFM image of the resulting Co MOLs. Reprinted with permission from Ref. [97], Copyright 2020, Elsevier.

common features of these parent MOFs are π-conjugated layered structures. The relatively weak interlayer interactions are conducive to the preferential orientation during MOL assembly.

Compared with liquid-liquid interface synthesis, liquid-gas interface synthesis can obtain thinner MOLs [107]. Nishihara and coworkers [99] used the liquid-liquid and liquid-air interface methods to synthesize bis(dipyrrinato)zinc(II) MOLs with different layers and sizes. Using the liquid-liquid interface method, they synthesized larger multilayer MOLs. Using the liquid-air interface method, they obtained monolayer MOLs. In the liquid-air interface synthesis, zinc acetate and ligand (**L1**) were first dispersed in H_2O and CH_2Cl_2, respectively. Then, CH_2Cl_2 of **L1** was slowly dispensed on the surface of the $Zn(OAc)_2$ aqueous solution. After CH_2Cl_2 was evaporated, **L1** and Zn^{2+} spontaneously complexed at the interface, and a single layer of MOLs was formed (Fig. 7). The optical and SEM images reveal a uniform, flat, film-like morphology.

The liquid-solid interface method was developed to synthesize 2D MOLs. Using this method, Kitagawa and coworkers [108] successfully synthesized $Fe(py)_2[Pt(CN)_4]$ (py = pyridine) MOLs.

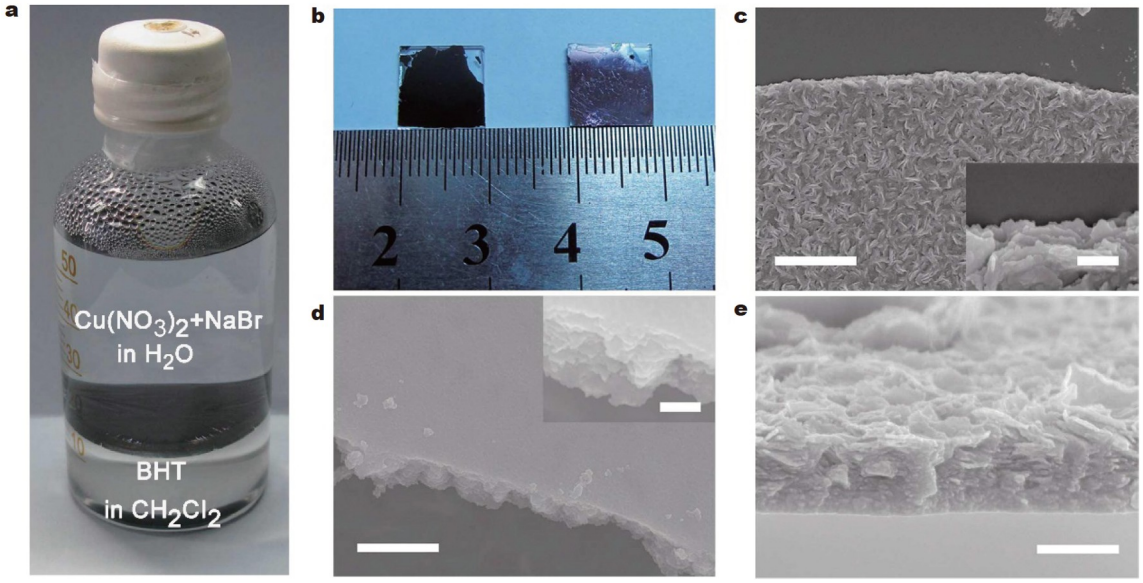

Figure 6 (a) Formation of Cu-BHT MOLs at the solution interface. (b) MOL films supported on glass substrates. SEM images of the (c) top and (d) bottom surfaces, as well as (e) the cross-section of Cu-BHT MOL film with a 200-nm thickness. The insets in (c) and (d) show detail of the film edge with enlarged scale. Scale bars are 200 nm for (d), 400 nm for (c, e), and 100 nm for the insets. Reprinted with permission from Ref. [71], Copyright 2016, Nature Publishing Group.

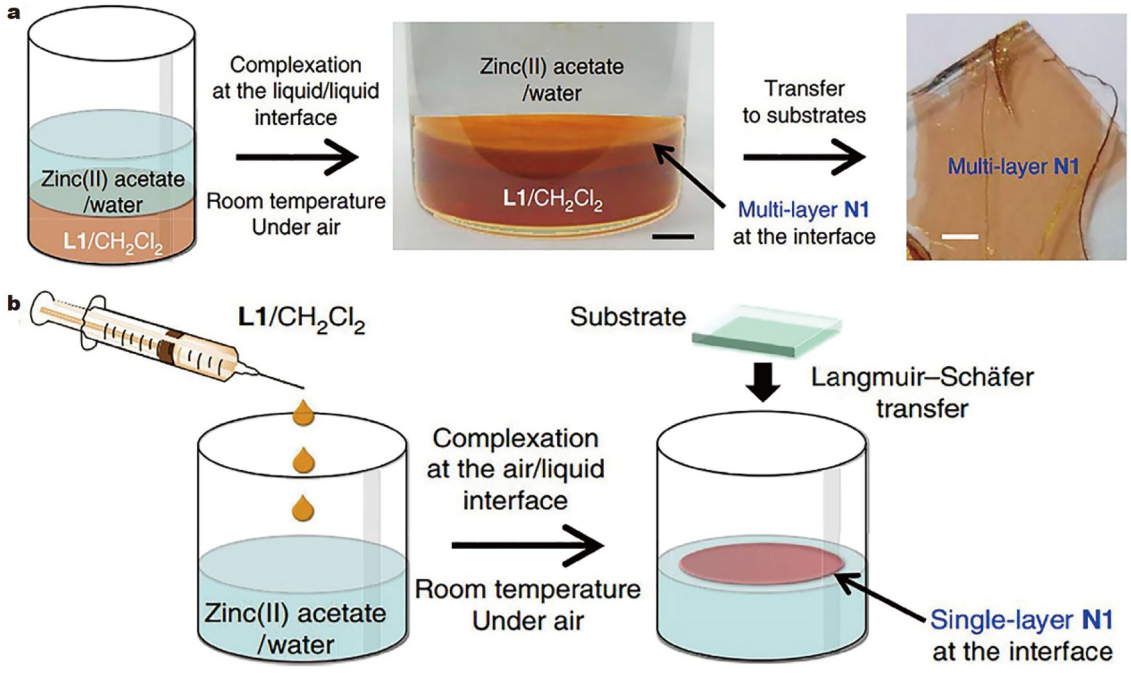

Figure 7 (a) Liquid-liquid and (b) liquid-air interfacial synthesis of bis(dipyrrinato)zinc(II) MOLs. Scale bars are 5 mm (middle) and 1 mm (right), respectively. Reprinted with permission from Ref. [99], Copyright 2015, Springer Nature.

First, they covered the Au/Cr/Si substrate with 4-mercaptopyridine to form a self-assembled monolayer. Then, the substrate was immersed alternately in Fe^{2+} and $[Pt(CN)_4]^{2-}$ ethanol solutions. After 30 cycles, the MOL film with a 16-nm thickness was obtained. Remarkably, through this method, the growth of the MOL film can be well regulated by the number of reaction cycles [109,110]. Zhuang and coworkers [111] fabricated microsupercapacitors (MSCs) using the LBL growth of a coordination polymer framework (PiCBA) on a Si-wafer-supported Au surface. The prepared MSCs exhibited alternating current line-filtering performance with a short resistance-capacitance constant of approximately 0.83 ms.

The previous discussions confirm that the interfacial method is beneficial for the syntheses of 2D ultrathin MOLs with large areas [104]. However, interfacial growth is not the general method for preparing 2D MOLs, which is usually suitable for MOFs with layered structures. Furthermore, the number of products is limited by the interfacial area; thus, the large-scale production of MOLs is probably impractical.

Direct solvothermal synthesis

Solvothermal synthesis is commonly used to prepare bulky MOF materials [13,112]. However, MOL materials obtained by direct solvothermal synthesis have not yet been reported until 2012, when Kitagawa and coworkers [113] stated that MOF nanofilms with perfect orientation and excellent crystallinity could be directly synthesized by the solvothermal reaction between Cu(II) and TCPP. By regulating the reaction conditions, the growth rates of different crystal facets in MOFs could be tuned. As such, MOF materials with different structures/morphologies could be obtained. If the MOF growth rate on the edge and in the vertical direction was different, then the crystal faces with a lower growth rate would tend to be exposed, which may facilitate the synthesis of MOLs [12].

Several research groups have successfully obtained MOLs using direct solvothermal methods [77,114–117]. For example, Jiang and coworkers [114] demonstrated the preparation of 3D hierarchical flower-like metal-organic materials (3D HFLM) *via* a one-pot solvothermal strategy, which features a unique hierarchical structure comprising 2D MOLs. The MOL was obtained *via* a solvothermal process using Co^{2+} and 2-methylimidazole (2-MeIm) as ingredients and methanol as a solution. Further solvothermal treatment and phosphorization led to the formation of CoM-P-3D HFLMs (M = Cu, Mn, Ni) (Fig. 8a). Lang and coworkers [77] synthesized a series of binary MOLs (Ni-M-MOF, M = Al, Mn, Fe, Co, Zn, or Cd) by direct synthesis (Fig. 8b). In this work, the solvent composition plays a critical role in modulating the MOL thickness and morphologies. This direct synthesis method can also be used to prepare 2D MOLs based on phthalocyanine ligands, as the interlayer π-π interactions in phthalocyanine-based MOFs can be weakened by certain solvents [116].

Furthermore, our group demonstrated the direct solvothermal syntheses of 2D Ni-MOLs [55]. Three MOF materials were obtained with $Ni(NO_3)_2{\cdot}6H_2O$ and H_2BDC as reactants, including the bulky Ni-MOF, Ni-MOL-100 exposing the (100) crystal facet, and Ni-MOL-010 exposing the (010) crystal facet (Fig. 8c). The Ni-MOF/MOLs can be used to catalyze the photochemical CO_2 reduction, and the activity of Ni-MOL-100 is 4.6 and 2.5 times higher than those of bulky Ni-MOF and Ni-MOL-010, respectively. The superior photocatalytic performance of Ni-MOL-100 can be ascribed to the synergistic catalysis of the adjacent Ni(II) ions with a close proximity of 3.50 Å, which provides more favorable energetics for CO_2 reduction with respect to that of Ni-MOL-010.

Direct solvothermal synthesis is remarkably convenient for the preparation of 2D MOLs. However, for some MOLs, using this method only leads to the formation of bulky MOFs. To inhibit the overgrowth of the MOLs, surfactant-assisted solvothermal synthesis was proposed by Zhang and coworkers [118,119]. They determined that the surfactants can adsorb onto the MOF surface selectively, which can control the growth of MOF, resulting in ultrathin Zn-TCPP nanosheets [120]. By contrast, in the absence of surfactants, the direct conventional synthesis only leads to the formation of bulky Zn-TCPP MOF (Fig. 9a). The obtained Zn-TCPP MOLs are 1.2 ± 0.4 μm in lateral size and 7.6 ± 2.6 nm in thickness, corresponding to the stacking of 8 ± 3 layers of Zn-TCPP assembled (Fig. 9b, c). With the same method, Zhang and coworkers [121] obtained another MOL based on porphyrin ligands (Fig. 9d). The square MOLs are uniform in lateral size (1.5 ± 0.3 μm) and thickness (42.7 ± 8.4 nm) (Fig. 9e, f).

Similar to surfactants, capping molecules are also helpful for the direct synthesis of MOLs. Lin and coworkers [122] reported the direct synthesis of Hf-based MOLs in the presence of formic acid. With the protection of formic acid, only six coplanar sites of the Hf_6 cluster with 12 connection sites can be connected to the benzene-1,3,5-tribenzoate (BTB) ligand. The 6-connected Hf_6 clusters and the 3-connected BTB together form a 2D 3,6-connected MOL. The powder X-ray diffraction (PXRD) pattern of the resulting MOL is consistent with that of the simulated bulky MOF. The wrinkled ultrathin MOLs are 4 mm × 4 mm in average lateral size and 2.2–3.2 nm in edge thickness, indicative of bilayer and trilayer structures. By partially substituting the BTB ligands with the 4′-(4-benzoate)-(2,2′,2″-terpyridine)-5,5″-dicarboxylate (TPY) ligands, a new MOL with the formula $[Hf_6(\mu_3\text{-}O)_4(\mu_3\text{-}OH)_4(HCO_2)_6(TPY)_2]$ was obtained [123], which has numerous uncoordinated N atoms at the MOL surface that enable further surface functionalization.

Sonochemical synthesis

In terms of sonochemical synthesis, on account of the rapid conventional solvothermal method, the reaction time needed for sonochemistry is short [124,125]. The resulting MOLs are approximately 3.1 nm in thickness, with numerous unsaturated active sites and large surface areas, thus, showing enhanced electrocatalytic oxygen evolution reaction (OER) performance. Moreover, other groups have used this approach to synthesize 2D MOLs from BDC ligands and a range of transition metal ions [51,126–130].

Template synthesis

Template synthesis has also been developed as a bottom-up approach to obtain 2D MOLs [50,66,131–134]. In 2019, Yao and coworkers [134] reported an MOF nanoarray ($Fe_{0.1}$-Ni-MOF/nickel foam (NF)), which was highly oriented and prepared by the *in situ* reaction. In this structure, both the nanoarray template and precursor are NiFe-layered dihydroxide nanoarray (NiFe-LDH/NF) on NF (Fig. 10a). During the reaction, the solutions of Fe^{3+} and Ni^{2+} ions were uniformly spread over both sides of the NiFe-LDH layer, which can serve as embedding sites for subsequent MOF self-assembly. The remaining NiFeO layer

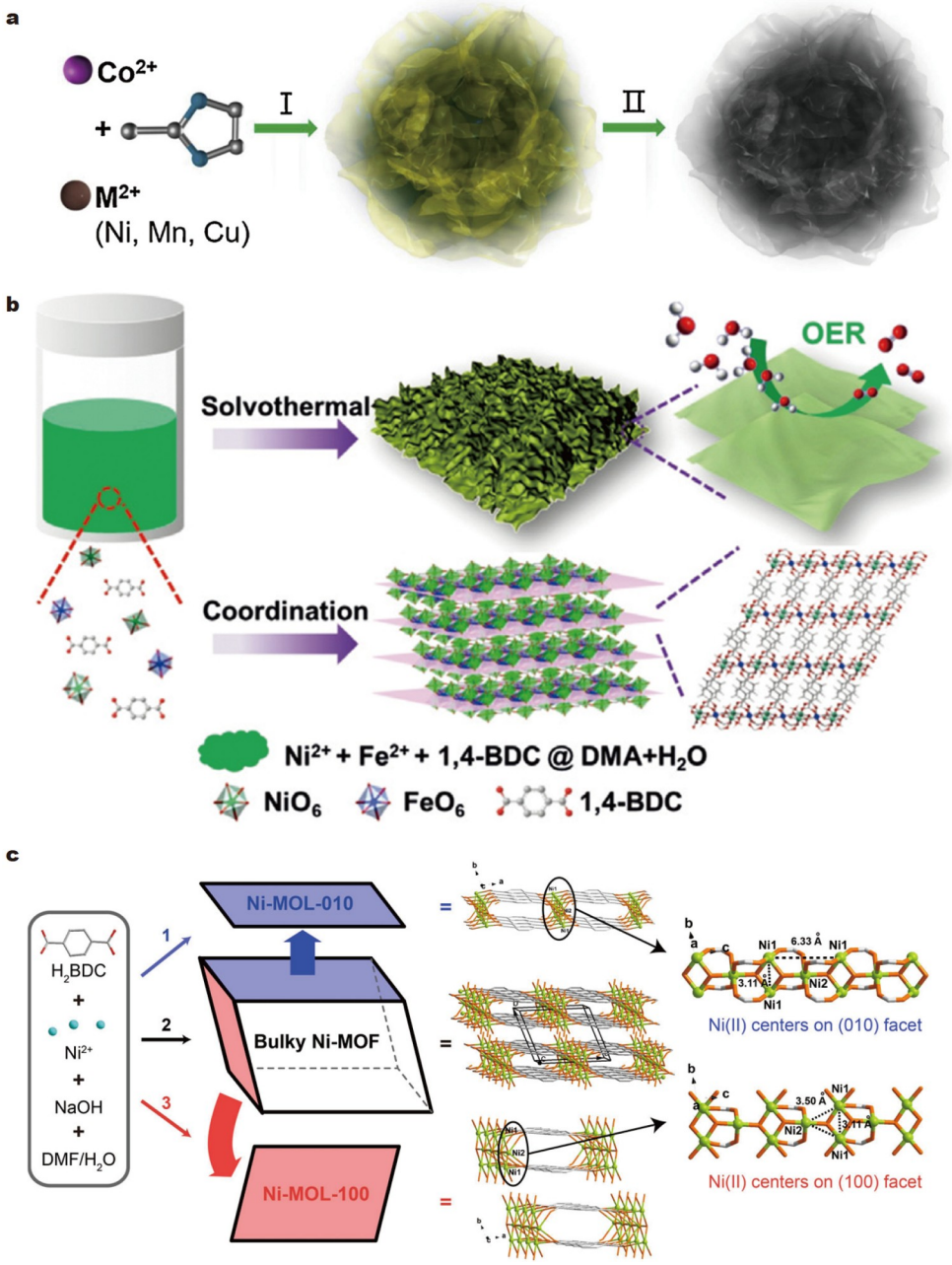

Figure 8 Direct solvothermal syntheses of (a) CoM-P-3DHFLMs (reprinted with permission from Ref. [114], Copyright 2019, Elsevier), (b) Ni-Fe-MOLs (reprinted with permission from Ref. [77], Copyright 2019, Wiley-VCH), and (c) Ni-MOF, Ni-MOL-010, and Ni-MOL-100 (reprinted with permission from Ref. [55], Copyright 2020, Wiley-VCH).

eventually transformed into uniform $Fe_{0.1}$-Ni-MOF [135]. Similarly, Ajayan and coworkers [132] utilized the sublimation-vapor phase pseudomorphic transformation (SVPT) approach for the template-assisted growth of MOLs (Fig. 10b). First, NiFe-LDH arrays were grown on NF. By increasing the reaction temperature, NiFe-LDH gradually transformed into nickel/iron oxides. With the temperature increased to 350°C, the formed nickel/iron oxides further reacted with the BDC ligand, *in situ* converting into 2D NiFe-MOLs supported on NF.

In addition to LDHs, metal oxides could also act as suitable precursors for the synthesis of 2D MOLs. Zhu and coworkers [136] used the amorphous M-ONS (M = Cu, Co, and Ni; ONS = oxide nanosheets) as the sacrifice template to react with the H_4dobdc ligand under hydrothermal conditions to form M-MNS by confined ligand coordination (Fig. 10c) [79]. In this way, the 2D single-metal MOF-74 and bimetal CoCu, NiFe, and FeCo-MOLs were synthesized. FeCo-MNS is 2.6 nm in thickness. This approach prevents the utilization of surfactants and enhances the interaction between active metal sites and substance molecules in catalysis, which makes it possible to synthesize a variety of 2D MOLs and their derivatives using diverse precursors and substrates.

Modulator-assisted synthesis

Modulator-assisted synthesis refers to control coordination equilibrium through a modulator that inhibits the deprotonation

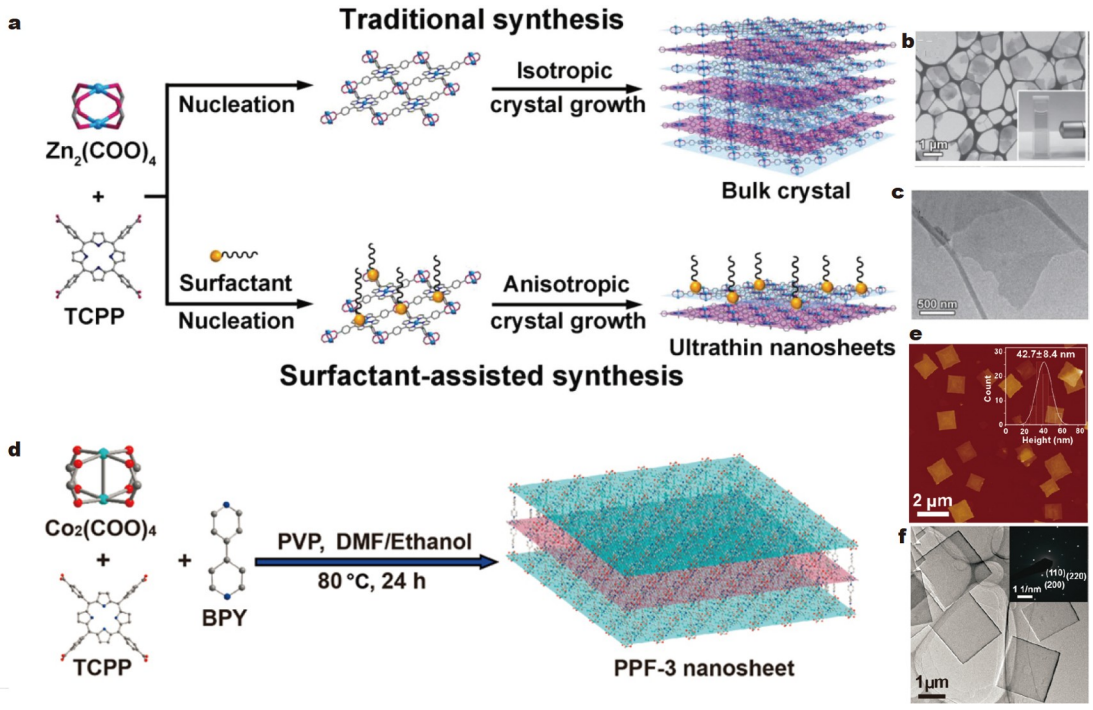

Figure 9 (a) Bulky MOFs and MOLs prepared by the traditional and surfactant-assisted methods, respectively. (b) Scanning TEM and (c) TEM images of Zn-TCPP MOLs. Inset: Tyndall effect of colloidal Zn-TCPP nanosheets in ethanol. Reprinted with permission from Ref. [120], Copyright 2015, Wiley-VCH. (d) Synthesis process of PPF-3 MOLs with polyvinyl pyrrolidone (PVP) assistance. (e) AFM image of PPF-3 nanosheets. Inset: Statistical analysis of the thickness of 75 PPF-3 nanosheets measured in AFM images. (f) TEM image of PPF-3 nanosheets. Inset: SAED pattern of PPF-3 nanosheets. Reprinted with permission from Ref. [121], Copyright 2016, American Chemical Society.

of the linker or competes with the ligand to coordinate with metal. The competitive effect reduces the rate of crystal growth and nucleation, which leads the MOFs to grow in a particular direction [137]. Small organic molecules, such as pyridine and acetic acid, are usually used as modulators to obtain 2D MOLs because of their unique role in limiting and regulating crystal growth by coordinating with metal ions [138–142]. In 2009, Kitagawa and coworkers [143] reported the modulator-assisted strategy to obtain nanorods, nanocubes, and MOLs (Fig. 11). Then, Do and coworkers [141] performed a pyridine modulator to synthesize 2D MOLs. Aside from small organic molecules, small inorganic molecules can also be used as modulators to obtain 2D MOLs. For instance, Nian and coworkers [144] used ammonia (NH_4OH) as a modulator to successfully synthesize 2D $Co_2(bim)_4$ MOLs.

Notably, both top-down and bottom-up methods are extensively employed by researchers to obtain MOL-based materials. Both methods have their advantages and disadvantages. The top-down method is simple but requires the advanced synthesis of 2D supramolecular precursors with weak interlayer supramolecular interactions. However, the morphology of the resulting MOLs, particularly the thickness, is difficult to control. By contrast, the bottom-up method is superior in controlling morphology, which can usually be achieved by tuning the reaction time. However, the yields are often unsatisfactory. Moreover, we cannot state that the bottom-up method is better than the top-down method. The selection of which method to use should be based on the specific MOFs and MOLs.

APPLICATIONS

With large surface areas, convenient means of mass transfer pathways, and highly dispersible metal active sites, 2D MOLs have demonstrated wide applications in gas separation, catalysis, energy conversion, and sensors.

Gas separation

Efficient gas separation of the ultrathin leachy membrane has attracted considerable attention because of its low energy consumption and excellent recyclability [16]. 2D materials, including carbonitrides, graphene, boron nitride, transition metal dihalides, and graphitized black phosphorus, have been developed as leachy membranes for gas separation [112,145]. In most instances, 2D materials are characterized as molecular sieves; thus, the gas macromolecules in the gas mixture do not pass through the membrane, and most small gas molecules can penetrate the channels, achieving highly selective gas separation [146]. In 2015, Cu-BDC nanosheets were combined with polyamide (PI) by Gascon and coworkers [76] to prepare composite membranes with a thickness of 30–50 nm. The obtained membrane showed excellent selectivity for CO_2/CH_4 separation. The higher occupation of the Cu-BDC MOLs than the bulk crystals leads to better separation of CO_2 and CH_4. At the same time, Yang and coworkers [70] have prepared 2D ultrathin MOLs of $Zn_2(bim)_4$ *via* the physical exfoliation method.

The obtained MOLs can serve as molecular sieves to efficiently separate H_2 and CO_2. By hot dropping $Zn_2(bim)_4$ MOLs glued to a porous leachy (α-Al_2O_3) disk, a composite membrane could be readily obtained. Control experiments demonstrated that the composite membrane obtained at 120°C showed excellent selectivity for the surface temperature. Three years later, the same group prepared another composite membrane from $Zn_2(bim)_3(OH)$ MOLs, which also exhibited superb capability to

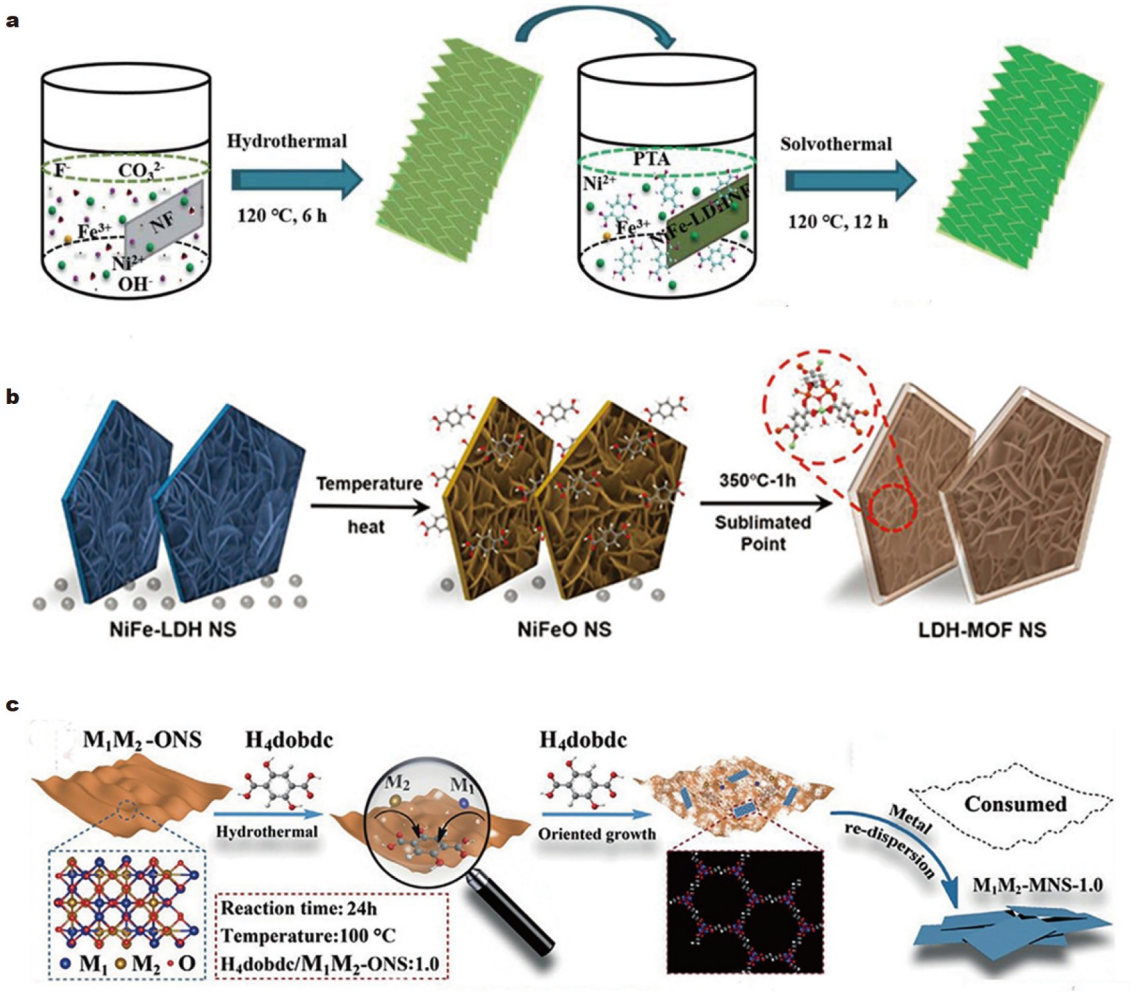

Figure 10 (a) Synthetic procedure of $Fe_{0.1}$-Ni-MOF/NF. Reprinted with permission from Ref. [134], Copyright 2019, Royal Society of Chemistry. (b) SVPT strategy used to prepare LDH-MOF MOLs. Reprinted with permission from Ref. [132], Copyright 2019, Wiley-VCH. (c) Preparation of M_1M_2-MNS-1.0 MOLs using metal oxides as sacrifice templates. Reprinted with permission from Ref. [79], Copyright 2019, Wiley-VCH.

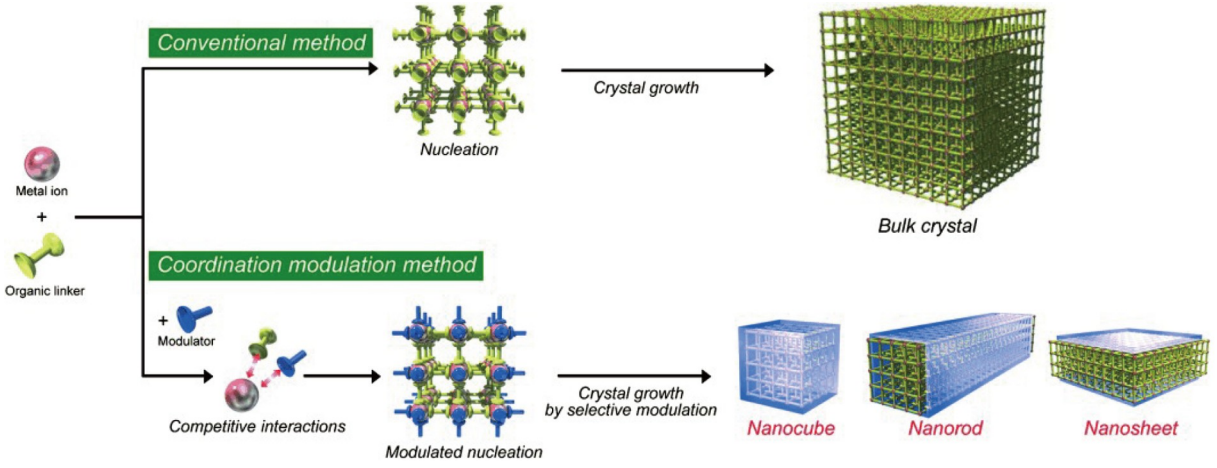

Figure 11 Traditional and coordination modulation methods for synthesizing MOF materials. Reprinted with permission from Ref. [143], Copyright 2009, Wiley-VCH.

separate H_2/CO_2 [87]. Apart from the dependence on pore separation, functional nodes and groups in MOLs can also be used to prepare MOL-based gas separation materials [42,56,84,147–150].

Catalysis

With numerous exposed active sites, 2D MOLs have also shown promising applications in catalysis as heterogeneous catalysts. Lin and coworkers [122] demonstrated that TPY-based Hf MOLs, after metalation with Fe^{2+} and activation by $NaBHEt_3$ (Fe-TPY MOLs), could catalyze styrene hydrosilylation (Fig. 12a).

When the loading amount of Fe-TPY MOLs was 0.02%, 100% conversion and selectivity of anti-Markovnikov products could be obtained within 48 h. By comparison, bulk MOF with interlocking structure did not transform, whereas bulk MOF with stacked structure produced only 30% of products. They further conducted surface modification on the TPY-based MOLs [123]. The modified MOLs showed good catalytic activity for the photocatalytic oxidation of THF into butyrolactone (BTL). The selectivity of GA-modified MOLs for BTL was 100%, whereas that of the unmodified MOLs for BTL was only 57.4%. For nearly all investigated organic reactions, 2D MOLs exhibited higher catalytic activity than those of their bulky counterparts [28,151–154]. Similar to their bulky counterparts, 2D MOLs could also be used as supports to immobilize metal nanoparticles (NPs) to form composite catalysts. Zhang and coworkers [119] obtained Au-NPs/Cu-TCPP(M) hybrid MOLs (M = Co/Fe) through the growth of Au-NPs on 2D metallic porphyrin MOLs. The obtained Au-NPs/Cu-TCPP(M) MOLs exhibited peroxidase-like and glucose oxidase (GOx)-like catalytic activities, catalyzing the oxidation of glucose to gluconic acid in the O_2 atmosphere (Fig. 12b). The afforded H_2O_2 could further oxidize TMB to oxTMB (TMB = 3,3′,5,5′-tetramethylbenzidine). A series of controlled experiments confirmed that Au-NPs/Cu-TCPP(M) MOLs catalyzed the oxidation of glucose to gluconic acid in the O_2 atmosphere (Fig. 12b). The obtained H_2O_2 could further oxidize TMB to oxTMB. A series of controlled experiments confirmed that Au-NPs/Cu-TCPP (M) MOLs could catalyze the cascade reaction.

Energy conversion

Photochemical, electrochemical, and photoelectrochemical hydrogen evolution reaction (HER), OER, oxygen reduction reaction (ORR), and CO_2 reduction reaction (CO_2RR) are typical energy conversion reactions currently investigated [155–161]. In this field, 2D MOL materials also show superiority over bulky MOLs because of the numerous active metal centers exposed on their interfaces [162–164].

For HER, in 2015, Feng and coworkers [104] prepared a 2D MOL made of nickel bis(dithiolene) coordination compound using the L-B method. The fabricated 2D NiTHT MOL, with a thickness of 0.7–0.9 nm, exhibited exceptional catalytic capability for HER. When the current density reaches 10 mA cm^{-2}, the Tafel slope and overpotential are only 80.5 mV dec^{-1} and 333 mV, respectively. Li *et al.* [165] built a hybrid nanostructure comprising CoP MOLs doped with metallic (Mn-CoP) (Fig. 13a). The MOLs can be used as high-performance catalysts for HER.

At 10 mA cm^{-2}, the onset overpotential of CoP MOLs is 75 mV, the Tafel slope is 61 mV dec^{-1}, and the overpotential is 148 mV in H_2SO_4 (0.5 mol L^{-1}). In alkaline KOH (1.0 mol L^{-1}), the onset overpotential is 110 mV, the Tafel slope is 85 mV dec^{-1}, and the overpotential is 195 mV (Fig. 13b–g).

For OER, 2D MOLs also showed satisfactory catalytic performance. Lang and coworkers [166] synthesized many rod-shaped Fe/Ni bimetallic MOF nanorods (Fe/Co/Ni(Mn)-MIL-53), which can be used as high-performance catalysts for OER. For Fe/Ni-MIL-53, Ni is treated as the active center. The addition of iron can move the Ni^{2+}/Ni^{3+} peak to a higher potential and improve the OER efficiency. In the catalysis process of

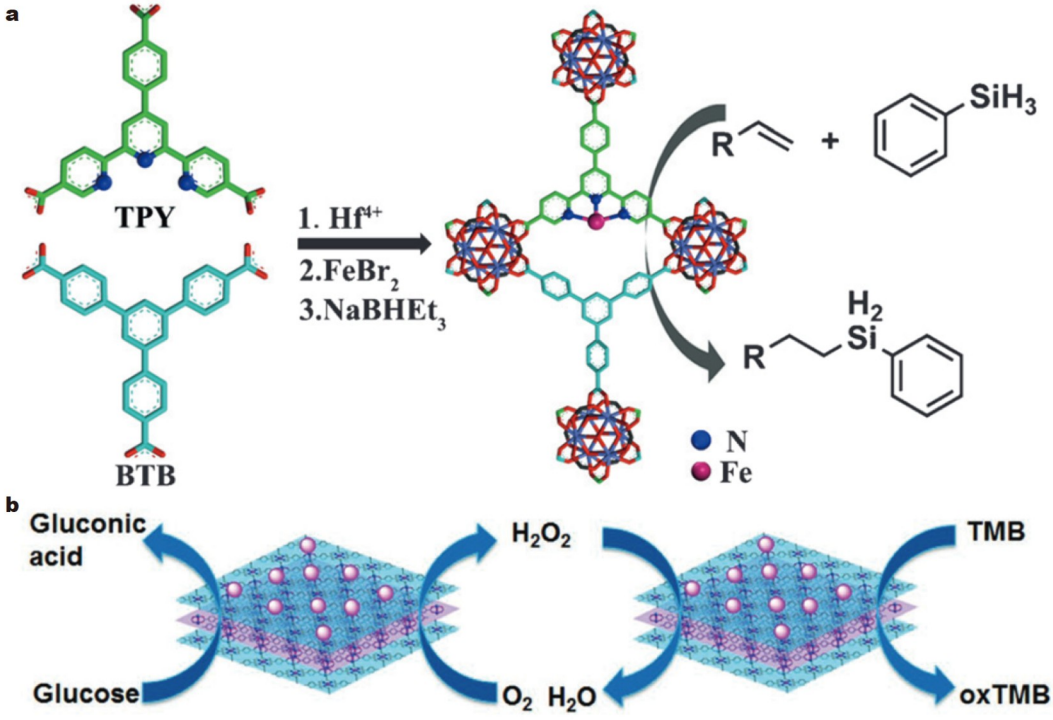

Figure 12 (a) Preparation of Fe-TPY MOLs and their catalytic performance. Reprinted with permission from Ref. [122], Copyright 2016, Wiley-VCH. (b) TMB oxidation by ultrathin Au-NPs/Cu-TCPP(M) hybrid MOLs. Reprinted with permission from Ref. [119], Copyright 2017, Wiley-VCH.

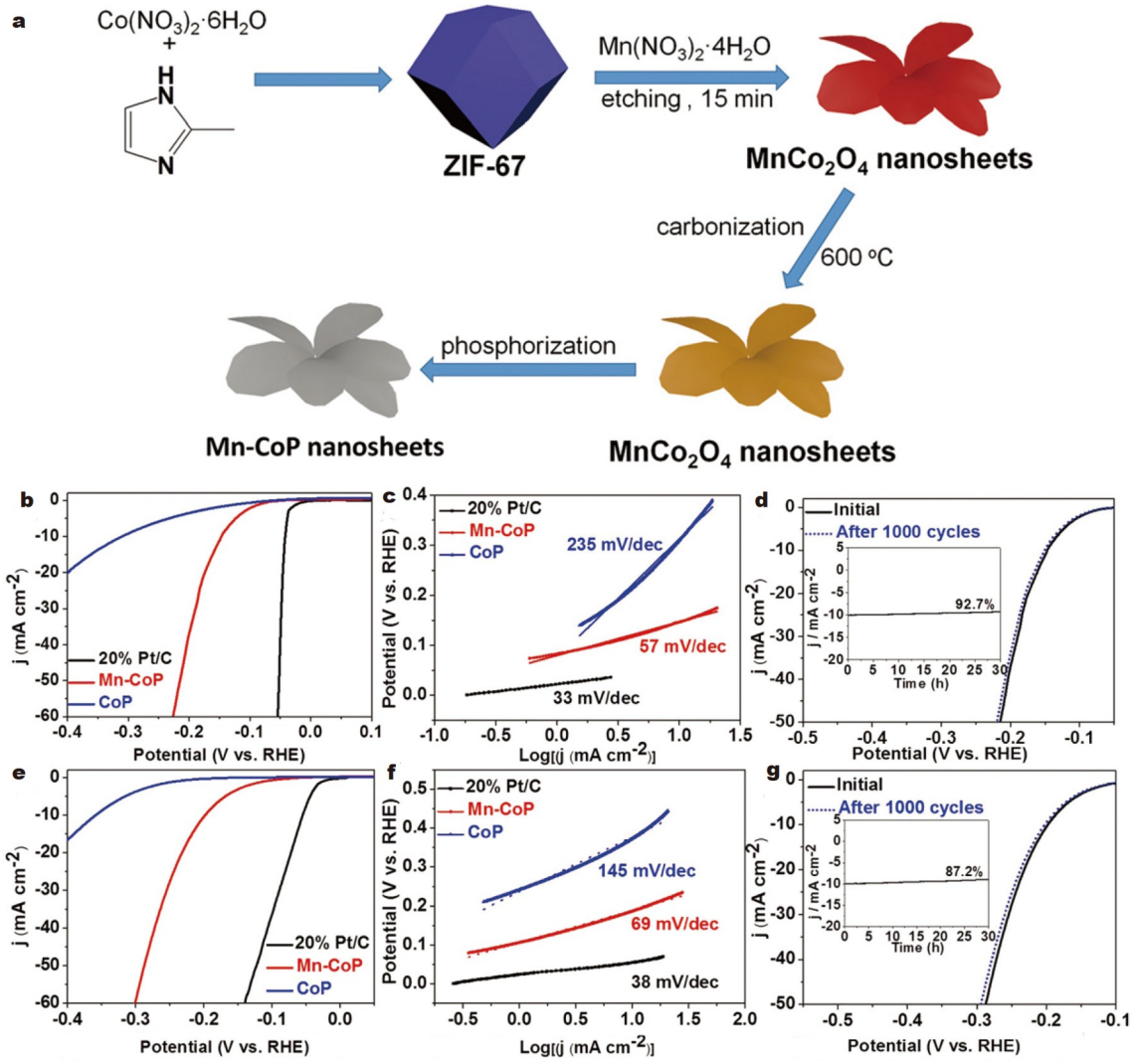

Figure 13 (a) Synthesis process of Mn-CoP MOLs. Linear sweep voltammetry (LSV) curves of hollow CoP, Mn-CoP MOLs, and Pt/C in (b) H_2SO_4 (0.5 mol L^{-1}) and (e) KOH (1.0 mol L^{-1}). Tafel curves of hollow CoP, Mn-CoP MOLs, and Pt/C in (c) H_2SO_4 (0.5 mol L^{-1}) and (f) KOH (1.0 mol L^{-1}). Stability tests for Mn-CoP MOLs in (d) H_2SO_4 (0.5 mol L^{-1}) and (g) KOH (1.0 mol L^{-1}). The insets in (d) and (g) show the corresponding time-dependent current density curves for the Mn-CoP nanosheet catalyst. Reprinted with permission from Ref. [165], Copyright 2018, The Royal Society of Chemistry.

$Fe/Ni_{2.4}/Co_{0.4}$-MIL-53, the overpotentials are 219 and 236 mV for 10 and 20 mA cm^{-2}, respectively. The Tafel slope is 53.5 mV dec^{-1}, which shows that these multimetal MOLs have good kinetic properties (Fig. 14a–e). Two years later, they used a bottom-up method to prepare binary Ni-M-MOLs (M = Al, Mn, Fe, Co, Zn, and Cd), which only have a thickness of a few atomic layers [77]. With the advantages of ultrathin thickness, exposed active sites, and fast electron transfer, the activity and durability of Ni-Fe-MOLs were significantly enhanced and better than most reported similar electrocatalysts [167,168]. At 10 mA cm^{-2}, the overpotential and Tafel slope are 221 mV and 56 mV dec^{-1}, respectively. Moreover, Ni-Fe-MOLs exhibit remarkable stability in electrocatalytic OER (Fig. 14f–i). The density functional theory (DFT) result supports that the excellent catalytic performance can be mainly attributed to more active Fe replacing Ni in Ni-Fe-MOLs.

Zhu and coworkers [79] synthesized FeCo-MNS, which shows a 298-mV overpotential and a 21.6 mV dec^{-1} Tafel slope at 10 mA cm^{-2} for electrocatalytic OER, superior to FeCo-ONS and Co-MNS (Fig. 15a–c). Such performance was inferred from the abundant metal sites on the FeCo-MNS surface and the synergistic catalysis between Fe and Co. In 2016, Tang and coworkers [126] demonstrated that ultrathin NiCo-MOLs, synthesized from Ni^{2+}, Co^{2+}, and BDC, have high OER electrocatalytic activity.

Under alkaline conditions, the overpotential of NiCo-MOLs on Cu foam was 250 mV to drive a current density of 10 mA cm^{-2}. It also exhibited high stability. During electrocatalysis for 200 h, the Faradaic efficiency reached 99.3%. Such high efficiency can be attributed to the synergy effect between Ni and Co.

Pang and coworkers [169] reported a series of 3D multilevel MOF hybrid materials. Under strongly alkaline conditions, the obtained hybrid materials exhibited superior catalytic activity for OER, with an overpotential of 195 mV at 10 mA cm^{-2}. Hou and coworkers [170] obtained Co/N-carbon nanosheet networks (CNSNs) using the hydrolysis and pyrolysis processes (Fig. 16a, b). Co/N-CNSNs exhibited not only OER catalytic activity but also ORR activity. At 10 mA cm^{-2}, a potential of 1.57 V was needed for Co/N-CNSNs in OER, which was lower

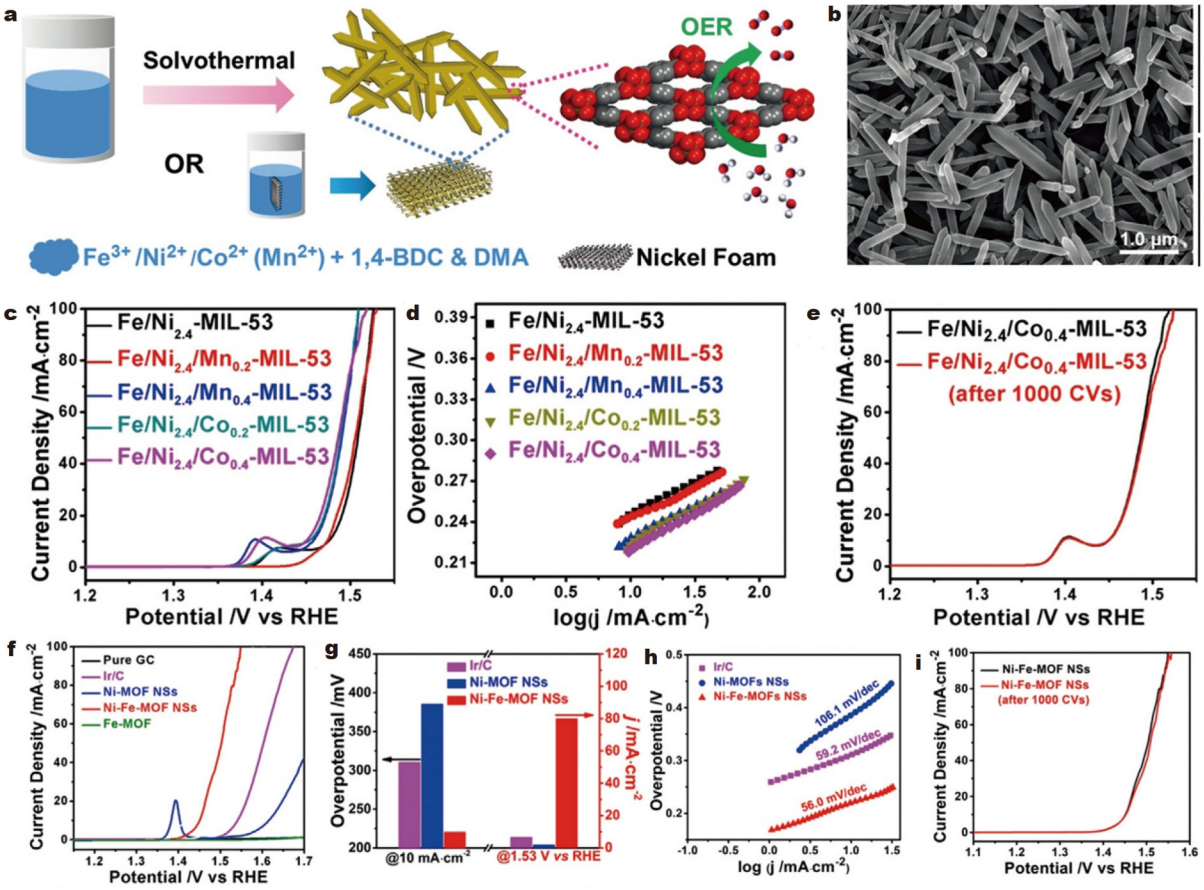

Figure 14 (a) Preparation process of Fe/Ni/Co(Mn)-MIL-53 and its OER performance. (b) Morphology of Fe/$Ni_{2.4}$/$Co_{0.4}$-MIL-53. (c) Polarization curves and (d) Tafel plots of Fe/$Ni_{2.4}$-MIL-53 and Fe/$Ni_{2.4}$/M_x-MIL-53. (e) Stability tests of Fe/$Ni_{2.4}$/$Co_{0.4}$-MIL-53. Reprinted with permission from Ref. [166], Copyright 2017, Wiley-VCH. (f) LSV curves of Ni-Fe-MOLs. (g) Overpotentials and current densities of different tested catalysts at 10 mA cm^{-2} and 1.53 V *vs.* reversible hydrogen electrode (RHE), respectively. (h) Tafel plots of Ni-Fe-MOLs and related catalysts. (i) Stability tests of Ni-Fe-MOLs. Reprinted with permission from Ref. [77], Copyright 2019, Wiley-VCH.

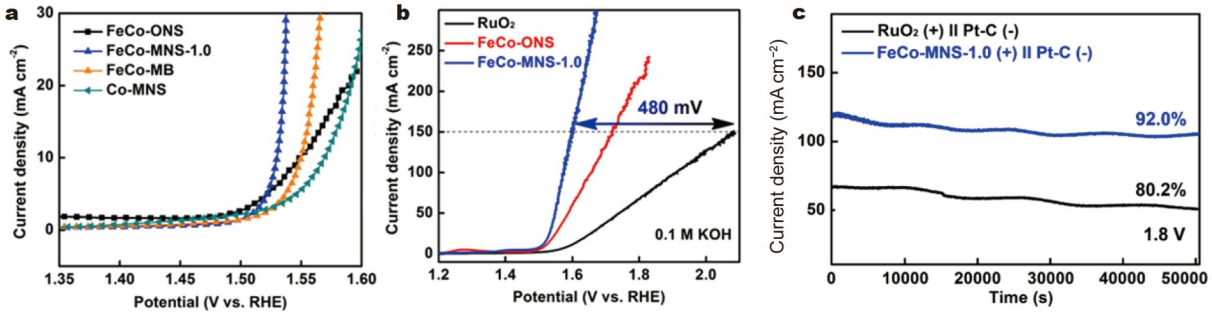

Figure 15 (a) OER polarization curves of FeCo-MOLs in KOH solution (0.1 mol L^{-1}). (b) OER curves of FeCo-MOLs loaded on NF in KOH solution (0.1 mol L^{-1}). (c) Continuous amperometric *i-t* measurements of FeCo-MOLs at 1.80 V in KOH solution (1.0 mol L^{-1}). Reprinted with permission from Ref. [79], Copyright 2019, Wiley-VCH.

than that for the catalysis of commercial IrO_2 (Fig. 16c–e). Jiang and coworkers [114] used the direct solvothermal synthesis method to obtain cobalt-based bimetallic phosphide nanosheets (CoM-P-3DHFLMs), which is a cost-effective OER electrocatalyst, having an overpotential of 292 mV at 10 mA cm^{-2} and durable stability for a catalytic period of approximately 10 h (Fig. 16f–h). At the same time, similar 2D MOLs with good electrocatalytic OER performance have also been reported by Lou's group [171].

For ORR, 2D MOLs can also serve as good electrocatalysts. Feng and coworkers [116] mixed PcCu-O_8-Co and carbon nanotubes to obtain a stable and active ORR electrocatalyst (PcCu-O_8-Co/CNTs). The half-wave potential ($E_{1/2}$) is 0.83 V *vs.* RHE, which is comparable to 0.85 V *vs.* RHE of commercial Pt/C.

For CO_2RR, many efforts have been devoted to the design and synthesis of catalysts with good catalytic performance [172–174]. Aside from homogeneous molecular catalysts, heterogeneous

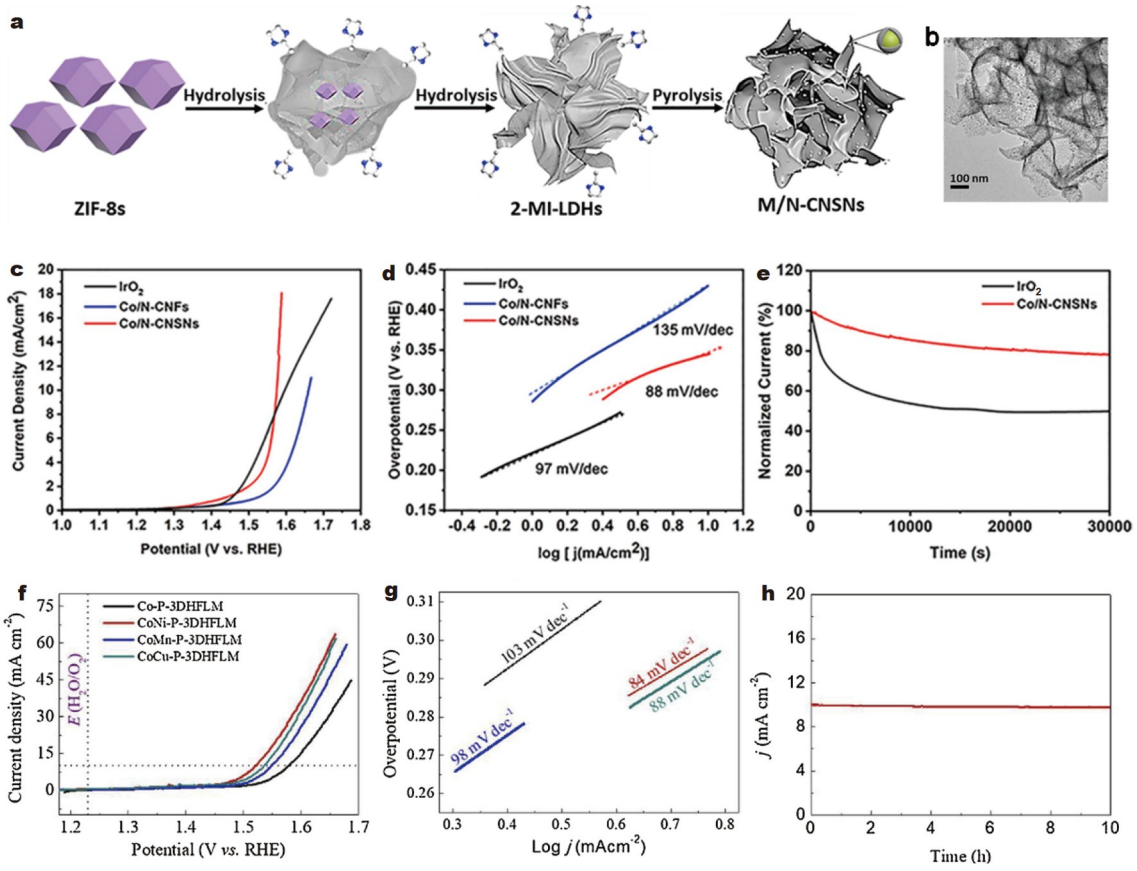

Figure 16 (a) Fabrication process of Co(Ni)/N-CNSNs. (b) Morphology of Co/N-CNSNs. (c) OER LSV curves and (d) Tafel plots of Co/N-CNSNs and related catalysts in 0.1 mol L^{-1} KOH solution saturated with O_2. (e) *i-t* responses in 0.1 mol L^{-1} KOH solution saturated with O_2. Reprinted with permission from Ref. [170], Copyright 2018, American Chemical Society. (f) OER LSV curves and (g) Tafel plots of CoM-P-3DHFLMs. (h) Stability test of CoNi-P-3DHFLM. Reprinted with permission from Ref. [114], Copyright 2019, Elsevier.

catalysts, including MOLs, have attracted considerable attention. For example, Sun and coworkers [173] used liquid phase epitaxy to deposit a monolithic, electrochemically efficient MOF thin film on a conductive FTO electrode. When used as an electrocatalyst for CO_2 reduction, this epitaxial surface grafted MOF (SURMOF) has a high Faradaic efficiency of 93% ± 5% for CO. Moreover, the current density is more than 2 mA cm^{-2}. Later, 2D ultrathin $Ni(Im)_2$ (Im = imidazole) MOLs were developed by Gu and coworkers [174] as electrocatalysts for CO_2RR. The $Ni(Im)_2$ MOLs were prepared by the ultrasonication of pristine $Ni(Im)_2$ crystals. Through different centrifugal forces, MOLs with different thicknesses can be obtained. The thickness of the thinnest MOLs is 5 nm, which has a Faradaic efficiency of 78.8% for CO.

The 2D planar feature of MOLs provides a good approach to analyze the influence of crystal facets on their catalytic performance. By controlling the reaction conditions of $Ni(NO_3)_2{\cdot}6H_2O$ and H_2BDC, we synthesized a bulky Ni-MOF and two Ni-MOLs, including Ni-MOL-100 exposing the (100) crystal facet and Ni-MOL-010 exposing the (010) crystal facet [55]. Further investigation showed that these materials can photocatalytically catalyze CO_2 reduction to CO. Ni-MOL-100 has higher activity than Ni-MOL-010 and bulky Ni-MOF (Fig. 17a–d). The DFT calculation revealed that the adjacent Ni sites within the (100) crystal facet can generate a synergistic catalysis effect, which endows Ni-MOL-100 with superior activity for CO_2-to-CO conversion.

Furthermore, we determined that MOLs can be used as precursors to prepare g-C_3N_4-based cost-efficient photocatalysts. Specifically, 2D ultrathin Co MOLs and urea were homogeneously mixed and then copyrolyzed, resulting in a series of single Co(II) site catalysts (g-C_3N_4-MOLs) [97]. The results of photocatalytic experiments show that g-C_3N_4-MOLs-30 has outstanding activity for the photocatalytic reduction of CO_2, with the CO yield rate as high as 464.1 μmol g^{-1} h^{-1} (Fig. 17e, f). In 2018, Lin and coworkers [51] constructed Ni-MOLs for the photoreduction of diluted CO_2. At 10% CO_2, Ni-MOLs show an apparent quantum yield of 1.96% and a CO selectivity of 96.8%, which is superior to reported systems in diluted CO_2 and exceeds most catalysts in pure CO_2 [175]. Zheng and coworkers [176] used Co MOLs as a precursor to prepare Co_3O_4 hierarchical nanosheets (Co_3O_4 HNSs) by calcination. The obtained Co_3O_4 inherits the 2D morphology of the parent MOLs. Thus, Co_3O_4 nanosheets have numerous mesoporous structures, good separation capacity, and large specific surface areas, with which the CO formation rate is 39.70 μmol h^{-1} in photochemical CO_2 reduction, higher than that of other Co_3O_4 nanoparticles.

Sensors

MOLs with functional groups are a promising platform for developing unique sensors [82,177]. Multitudinous MOLs applied to sensors have been reported. Qian and coworkers [178] reported a 2D MOL (NTU-9-NS) based on $Ti_2(HDOBDC)_2$

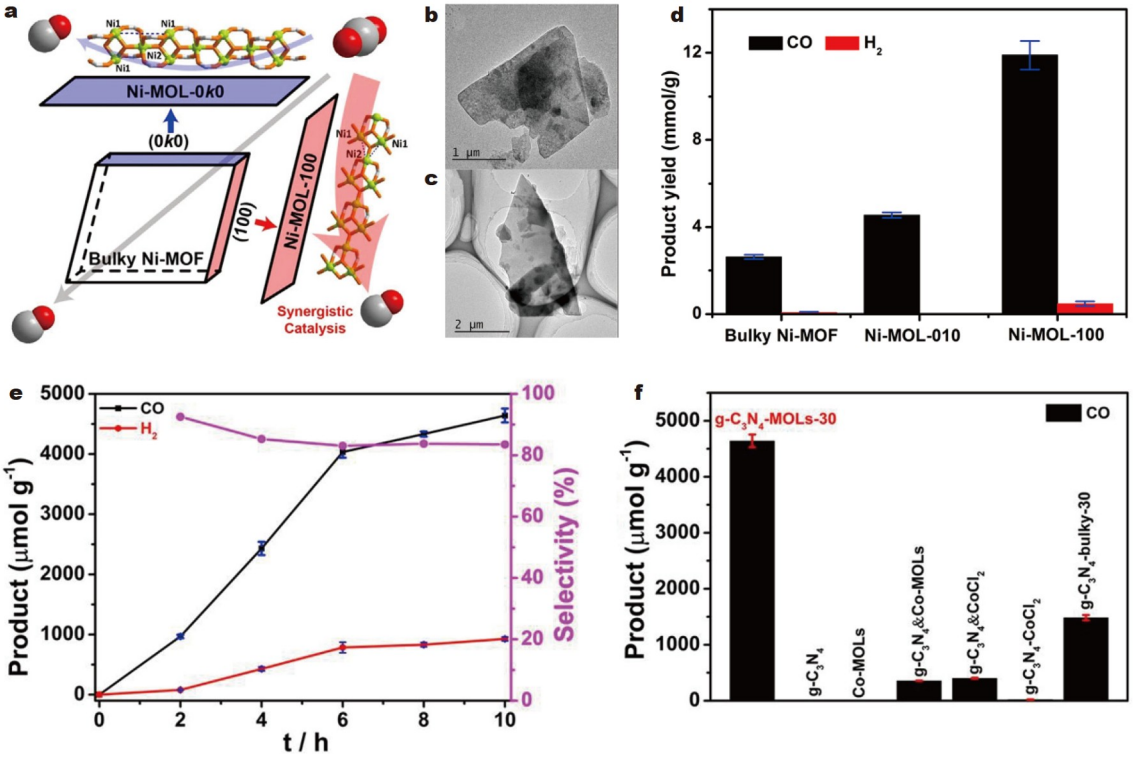

Figure 17 (a) Synthesis strategy for bulky Ni-MOF, as well as Ni-MOLs exposing the (010) and (100) crystal facets. TEM images for Ni-MOL exposing the (b) (010) and (c) (100) crystal facets. (d) Photocatalytic CO_2 reduction activities of bulky Ni-MOF, as well as Ni-MOLs exposing the (010) and (100) crystal facets. Reprinted with permission from Ref. [55], Copyright 2020, Wiley-VCH. (e) Photocatalytic CO_2 reduction activity of g-C_3N_4-MOLs-30. (f) Photocatalytic CO_2 reduction activities of g-C_3N_4-MOLs-30 and related catalysts. Reprinted with permission from Ref. [97], Copyright 2020, Elsevier.

(H_2DOBDC) (NTU-9), which shows high sensitivity to Fe^{3+}. The active sites located on the MOL surface can be in close contact with Fe^{3+} ions. Zhang and coworkers [120] developed Cu-TCPP MOLs to test ssDNA and dsDNA in 2015. They determined that Cu-TCPP MOLs showed a low detection limit for the H_5N_1 gene, which is far lower than that of MOF particles. Furthermore, by designing the reaction system and adding ligands or other small guest molecules, the obtained MOLs can be applied to the fluorescence emitters of various analytes. Li and coworkers [179] fabricated a luminescent MOL with a thickness of 4 nm, which can act as a fluorescent sensor for H_2O_2 *via* a quenching mechanism with a detection limit of 0.87 μmol L^{-1}. Zhang and coworkers [118] prepared a series of ultrathin M-TCPP(Fe) MOLs with a thickness of 10 nm. Through the Langmuir-Schäfer deposition method, these MOLs can be supported on electrodes for H_2O_2 sensing. The results showed that MOLs have better water dispersion and more accessible active sites, which is better than bulk MOF in bionic catalysis. Subsequently, other luminescent MOLs with good performance in sensors were obtained [38,180–185].

Others

The applications of 2D MOLs have also been explored in artificial enzymes [119], enzyme inhibitors [39], and other fields. In 2017, Zhou and coworkers [39] developed 2D Cu-MOLs, which can be used as valid enzyme inhibitors and provide a novel means to understand the relationship between MOF and enzyme. The regulation of enzyme activity by 2D MOLs opens up new opportunities.

SUMMARY AND OUTLOOKS

In summary, we specifically reviewed the recent advances in the preparation and applications of 2D MOLs. In the preparation section, two methods, namely, bottom-up and top-down, have been introduced and discussed in detail. Within both methods, several strategies have been conceived and developed by researchers, aiming at the controlled preparation of MOLs with the desired sizes and thicknesses. Subsequently, many 2D MOLs have been successfully obtained. In the application section, the potential applications of MOLs in separation, catalysis, energy conversion, and sensors have been summarized and discussed.

The rapid development of 2D MOLs has demonstrated that MOLs are a new type of promising MOF-derived materials. Because of their numerous active sites, large specific surface areas, and facility for mass transfer, the applications of 2D MOLs can be further expanded from their parent bulky MOFs, particularly in separation, catalysis, and energy conversion. However, as a type of emerging multifunctional material, the investigation of 2D MOLs still faces some significant challenges. Thus, the widespread applications of 2D MOLs are still in their infancy. (1) Although a diverse range of strategies have been developed, the one capable of producing homogeneous MOLs on a large scale has not yet been reported. As the performance of MOLs is closely related to their thickness, a more practical and effective preparation method to improve the yield of 2D MOLs with a certain thickness is much desired. In this regard, we developed a ligand replacement route to produce monolayer MOLs from 3D MOF precursors [72]. This approach is based on the coordination chemistry theory. By replacing weaker coordinating pillar

ligands with stronger coordinating capping ligands, MOLs with certain thicknesses could be easily obtained by tuning the reaction time. With this method, we obtained MOLs with uniform morphology and single-layer thickness on a large scale. Moreover, the combination of two stripping methods was determined to be more effective in accelerating the exfoliation of bulky MOFs. For instance, the stripping rate of MOFs through the combination of chemical stripping and intercalation can be considerably improved [94]. Moreover, surfactants can be added in direct solvothermal synthesis to obtain high-quality 2D MOLs [120]. (2) Current characterization methods, including PXRD, SEM, and TEM, can provide morphological and rough structural information on MOLs. However, these analysis means cannot provide definite surface compositions and structures of MOLs. The structures of nearly all reported MOLs are unclear. Thus, the development of reliable characterization methods for directly observing the structures of MOLs, which will be beneficial for obtaining real structure-performance relationships, is necessary. At this point, the well-known electron diffraction technique and X-ray absorption spectroscopy may provide opportunities to reveal the MOL structures. (3) Current studies of the applications of MOLs are usually conducted from a macroscopic perspective. As a type of nanomaterial with one growth direction constrained, the nanosize effect exists in MOLs in contrast to their bulky counterparts. This effect would endow MOLs with particular functionalities compared with their bulky parents. From this point, the applications of MOLs could be significantly extended. Overall, as a type of emerging material, some significant challenges will be encountered. With the development of advanced characterization techniques and in-depth investigations on MOLs, we believe that these problems could be solved and the applications of MOLs could be further explored and extended in the future.

Received 23 September 2022; accepted 4 November 2022; published online 18 January 2023

1 Furukawa H, Cordova KE, O'Keeffe M, *et al.* The chemistry and applications of metal-organic frameworks. Science, 2013, 341: 1230444
2 Han Y, Li JR, Xie Y, *et al.* Substitution reactions in metal-organic frameworks and metal-organic polyhedra. Chem Soc Rev, 2014, 43: 5952–5981
3 Zhou HC, Long JR, Yaghi OM. Introduction to metal-organic frameworks. Chem Rev, 2012, 112: 673–674
4 Yaghi OM, Li G, Li H. Selective binding and removal of guests in a microporous metal-organic framework. Nature, 1995, 378: 703–706
5 Jiang W, Wang H, Zhang X, *et al.* Two-dimensional polymeric carbon nitride: Structural engineering for optimizing photocatalysis. Sci China Chem, 2018, 61: 1205–1213
6 Lin ZJ, Lü J, Hong M, *et al.* Metal-organic frameworks based on flexible ligands (FL-MOFs): Structures and applications. Chem Soc Rev, 2014, 43: 5867–5895
7 Taddei M. When defects turn into virtues: The curious case of zirconium-based metal-organic frameworks. Coord Chem Rev, 2017, 343: 1–24
8 Wang Q, Astruc D. State of the art and prospects in metal-organic framework (MOF)-based and MOF-derived nanocatalysis. Chem Rev, 2020, 120: 1438–1511
9 Yin H, Tang Z. Ultrathin two-dimensional layered metal hydroxides: An emerging platform for advanced catalysis, energy conversion and storage. Chem Soc Rev, 2016, 45: 4873–4891
10 Zhao Y, Liu J, Horn M, *et al.* Recent advancements in metal organic framework based electrodes for supercapacitors. Sci China Mater, 2018, 61: 159–184
11 Della Rocca J, Liu D, Lin W. Nanoscale metal-organic frameworks for biomedical imaging and drug delivery. Acc Chem Res, 2011, 44: 957–968
12 Carné A, Carbonell C, Imaz I, *et al.* Nanoscale metal-organic materials. Chem Soc Rev, 2011, 40: 291–305
13 Ma S, Cai M, Cheng T, *et al.* Two-dimensional organic-inorganic hybrid perovskite: From material properties to device applications. Sci China Mater, 2018, 61: 1257–1277
14 Wang S, McGuirk CM, d'Aquino A, *et al.* Metal-organic framework nanoparticles. Adv Mater, 2018, 30: 1800202
15 Kim S, Wang H, Lee YM. 2D nanosheets and their composite membranes for water, gas, and ion separation. Angew Chem Int Ed, 2019, 58: 17512–17527
16 Liu J, Yu H, Wang L, *et al.* Two-dimensional metal-organic frameworks nanosheets: Synthesis strategies and applications. Inorg Chim Acta, 2018, 483: 550–564
17 Wang J, Li N, Xu Y, *et al.* Two-dimensional MOF and COF nanosheets: Synthesis and applications in electrochemistry. Chem Eur J, 2020, 26: 6402–6422
18 Zhao M, Huang Y, Peng Y, *et al.* Two-dimensional metal-organic framework nanosheets: Synthesis and applications. Chem Soc Rev, 2018, 47: 6267–6295
19 Zhao P, Jian M, Zhang Q, *et al.* A new paradigm of ultrathin 2D nanomaterial adsorbents in aqueous media: Graphene and GO, MoS_2, MXenes, and 2D MOFs. J Mater Chem A, 2019, 7: 16598–16621
20 Dong R, Zhang T, Feng X. Interface-assisted synthesis of 2D materials: Trend and challenges. Chem Rev, 2018, 118: 6189–6235
21 Duan J, Li Y, Pan Y, *et al.* Metal-organic framework nanosheets: An emerging family of multifunctional 2D materials. Coord Chem Rev, 2019, 395: 25–45
22 Xiao X, Zou L, Pang H, *et al.* Synthesis of micro/nanoscaled metal-organic frameworks and their direct electrochemical applications. Chem Soc Rev, 2020, 49: 301–331
23 Xu M, Yang SS, Gu ZY. Two-dimensional metal-organic framework nanosheets: A rapidly growing class of versatile nanomaterials for gas separation, MALDI-TOF matrix and biomimetic applications. Chem Eur J, 2018, 24: 15131–15142
24 Zhao W, Peng J, Wang W, *et al.* Ultrathin two-dimensional metal-organic framework nanosheets for functional electronic devices. Coord Chem Rev, 2018, 377: 44–63
25 Zhao M, Lu Q, Ma Q, *et al.* Two-dimensional metal-organic framework nanosheets. Small Methods, 2017, 1: 1600030
26 Abhervé A, Mañas-Valero S, Clemente-León M, *et al.* Graphene related magnetic materials: Micromechanical exfoliation of 2D layered magnets based on bimetallic anilate complexes with inserted $[Fe^{III}(acac_2\text{-trien})]^+$ and $[Fe^{III}(sal_2\text{-trien})]^+$ molecules. Chem Sci, 2015, 6: 4665–4673
27 Coleman JN, Lotya M, O'Neill A, *et al.* Two-dimensional nanosheets produced by liquid exfoliation of layered materials. Science, 2011, 331: 568–571
28 Ding Y, Chen YP, Zhang X, *et al.* Controlled intercalation and chemical exfoliation of layered metal-organic frameworks using a chemically labile intercalating agent. J Am Chem Soc, 2017, 139: 9136–9139
29 Dou JH, Sun L, Ge Y, *et al.* Signature of metallic behavior in the metal-organic frameworks M_3(hexaiminobenzene)$_2$ (M = Ni, Cu). J Am Chem Soc, 2017, 139: 13608–13611
30 Kondo A, Kajiro H, Noguchi H, *et al.* Super flexibility of a 2D Cu-based porous coordination framework on gas adsorption in comparison with a 3D framework of identical composition: framework dimensionality-dependent gas adsorptivities. J Am Chem Soc, 2011, 133: 10512–10522
31 Motoyama S, Makiura R, Sakata O, *et al.* Highly crystalline nanofilm by layering of porphyrin metal-organic framework sheets. J Am Chem Soc, 2011, 133: 5640–5643
32 Sheberla D, Sun L, Blood-Forsythe MA, *et al.* High electrical conductivity in Ni_3(2,3,6,7,10,11-hexaiminotriphenylene)$_2$, a semiconducting metal-organic graphene analogue. J Am Chem Soc, 2014, 136: 8859–8862

33 Tan JC, Saines PJ, Bithell EG, *et al.* Hybrid nanosheets of an inorganic-organic framework material: Facile synthesis, structure, and elastic properties. ACS Nano, 2012, 6: 615–621
34 Coleman JN. Liquid exfoliation of defect-free graphene. Acc Chem Res, 2013, 46: 14–22
35 Chandrasekhar P, Mukhopadhyay A, Savitha G, *et al.* Orthogonal self-assembly of a trigonal triptycene triacid: Signaling of exfoliation of porous 2D metal-organic layers by fluorescence and selective CO_2 capture by the hydrogen-bonded MOF. J Mater Chem A, 2017, 5: 5402–5412
36 Huang J, Li Y, Huang RK, *et al.* Electrochemical exfoliation of pillared-layer metal-organic framework to boost the oxygen evolution reaction. Angew Chem Int Ed, 2018, 57: 4632–4636
37 Kambe T, Sakamoto R, Hoshiko K, *et al.* π-conjugated nickel bis(dithiolene) complex nanosheet. J Am Chem Soc, 2013, 135: 2462–2465
38 Wang HS, Li J, Li JY, *et al.* Lanthanide-based metal-organic framework nanosheets with unique fluorescence quenching properties for two-color intracellular adenosine imaging in living cells. NPG Asia Mater, 2017, 9: e354
39 Xu M, Yuan S, Chen XY, *et al.* Two-dimensional metal-organic framework nanosheets as an enzyme inhibitor: Modulation of the α-chymotrypsin activity. J Am Chem Soc, 2017, 139: 8312–8319
40 Zheng H, Huang S, Luo M, *et al.* Photochemical *in situ* exfoliation of metal-organic frameworks for enhanced visible-light-driven CO_2 reduction. Angew Chem Int Ed, 2020, 59: 23588–23592
41 Kondo A, Noguchi H, Carlucci L, *et al.* Double-step gas sorption of a two-dimensional metal-organic framework. J Am Chem Soc, 2007, 129: 12362–12363
42 Ang H, Hong L. Polycationic polymer-regulated assembling of 2D MOF nanosheets for high-performance nanofiltration. ACS Appl Mater Interfaces, 2017, 9: 28079–28088
43 Cao L, Lin Z, Shi W, *et al.* Exciton migration and amplified quenching on two-dimensional metal-organic layers. J Am Chem Soc, 2017, 139: 7020–7029
44 Feng D, Gu ZY, Li JR, *et al.* Zirconium-metalloporphyrin PCN-222: Mesoporous metal-organic frameworks with ultrahigh stability as biomimetic catalysts. Angew Chem Int Ed, 2012, 51: 10307–10310
45 He C, Lu K, Liu D, *et al.* Nanoscale metal-organic frameworks for the Co-delivery of cisplatin and pooled siRNAs to enhance therapeutic efficacy in drug-resistant ovarian cancer cells. J Am Chem Soc, 2014, 136: 5181–5184
46 Zhang J, Chen Y, Wang X. Two-dimensional covalent carbon nitride nanosheets: Synthesis, functionalization, and applications. Energy Environ Sci, 2015, 8: 3092–3108
47 Xiao Y, Chen C, Wu Y, *et al.* Fabrication of two-dimensional metal-organic framework nanosheets through crystal dissolution-growth kinetics. ACS Appl Mater Interfaces, 2022, 14: 7192–7199
48 Ren X, Liu W, Zhou H, *et al.* Biodegradable 2D GeP nanosheets with high photothermal conversion efficiency for multimodal cancer theranostics. Chem Eng J, 2022, 431: 134176
49 Deng C, Gao Y, Yao Y, *et al.* Conversion of layered materials to ultrathin amorphous nanosheets induced by ball-milling insertion and pure-water exfoliation. J Mater Chem A, 2022, 10: 11766–11773
50 Niu K, Xu Y, Wang H, *et al.* A spongy nickel-organic CO_2 reduction photocatalyst for nearly 100% selective CO production. Sci Adv, 2017, 3: e1700921
51 Han B, Ou X, Deng Z, *et al.* Nickel metal-organic framework monolayers for photoreduction of diluted CO_2: Metal-node-dependent activity and selectivity. Angew Chem Int Ed, 2018, 57: 16811–16815
52 Hu S, Yan J, Huang X, *et al.* A sensing platform for hypoxanthine detection based on amino-functionalized metal organic framework nanosheet with peroxidase mimic and fluorescence properties. Sens Actuat B-Chem, 2018, 267: 312–319
53 Kornienko N, Zhao Y, Kley CS, *et al.* Metal-organic frameworks for electrocatalytic reduction of carbon dioxide. J Am Chem Soc, 2015, 137: 14129–14135
54 Maka VK, Mukhopadhyay A, Savitha G, *et al.* Fluorescent 2D metal-organic framework nanosheets (MONs): Design, synthesis and sensing of explosive nitroaromatic compounds (NACs). Nanoscale, 2018, 10: 22389–22399
55 Yang W, Wang HJ, Liu RR, *et al.* Tailoring crystal facets of metal-organic layers to enhance photocatalytic activity for CO_2 reduction. Angew Chem Int Ed, 2021, 60: 409–414
56 Zou C, Li Q, Cheng F, *et al.* Homochiral porous coordination polymers with a rare utk topology and two types of uniform channels for enantioseparation. CrystEngComm, 2017, 19: 2718–2722
57 Peng X, Pelz PM, Zhang Q, *et al.* Observation of formation and local structures of metal-organic layers *via* complementary electron microscopy techniques. Nat Commun, 2022, 13: 5197
58 Xia D, Sun K, Zeng Y, *et al.* The organic bromide sources adjusting the shape and band structures of BiOBr nanosheets for enhanced photodegradation performances of BPA. Catalysts, 2022, 12: 820
59 Yang X, Shi Y, Xie K, *et al.* Cocrystallization enabled spatial self-confinement approach to synthesize crystalline porous metal oxide nanosheets for gas sensing. Angew Chem Int Ed, 2022, 61: e202207816
60 Zeng T, Meng X, Huang H, *et al.* Controllable synthesis of web-footed PdCu nanosheets and their electrocatalytic applications. Small, 2022, 18: 2107623
61 Yu T, Wang Y, Jiang K, *et al.* Catechol-coordinated framework film-based micro-supercapacitors with AC line filtering performance. Chem Eur J, 2021, 27: 6340–6347
62 Wang H, Qiu F, Lu C, *et al.* A terpyridine-Fe^{2+}-based coordination polymer film for on-chip micro-supercapacitor with AC line-filtering performance. Polymers, 2021, 13: 1002
63 Pan L, Jiang K, Zhai G, *et al.* A novel 2D conjugated coordination framework with a narrow bandgap for micro-supercapacitors. Energy Tech, 2022, 10: 2200133
64 Yang H, Zhao Y, Chen Z, *et al.* A narrow bandgap, isocyanide-based coordination polymer framework for micro-supercapacitors with AC line-filtering performance. Macro Chem Phys, 2022, 223: 2200037
65 Novoselov KS, Geim AK, Morozov SV, *et al.* Electric field effect in atomically thin carbon films. Science, 2004, 306: 666–669
66 Huang X, Qi X, Boey F, *et al.* Graphene-based composites. Chem Soc Rev, 2012, 41: 666–686
67 Tan C, Cao X, Wu XJ, *et al.* Recent advances in ultrathin two-dimensional nanomaterials. Chem Rev, 2017, 117: 6225–6331
68 Nielsen RB, Kongshaug KO, Fjellvåg H. Delamination, synthesis, crystal structure and thermal properties of the layered metal-organic compound $Zn(C_{12}H_{14}O_4)$. J Mater Chem, 2008, 18: 1002–1007
69 Makiura R, Motoyama S, Umemura Y, *et al.* Surface nano-architecture of a metal-organic framework. Nat Mater, 2010, 9: 565–571
70 Peng Y, Li Y, Ban Y, *et al.* Metal-organic framework nanosheets as building blocks for molecular sieving membranes. Science, 2014, 346: 1356–1359
71 Huang X, Sheng P, Tu Z, *et al.* A two-dimensional π-d conjugated coordination polymer with extremely high electrical conductivity and ambipolar transport behaviour. Nat Commun, 2015, 6: 7408
72 Deng JH, Wen YQ, Willman J, *et al.* Facile exfoliation of 3D pillared metal-organic frameworks (MOFs) to produce MOF nanosheets with functionalized surfaces. Inorg Chem, 2019, 58: 11020–11027
73 Kang Z, Fan L, Sun D. Recent advances and challenges of metal-organic framework membranes for gas separation. J Mater Chem A, 2017, 5: 10073–10091
74 Jiang Q, Zhou C, Meng H, *et al.* Two-dimensional metal-organic framework nanosheets: Synthetic methodologies and electrocatalytic applications. J Mater Chem A, 2020, 8: 15271–15301
75 Li Y, Fu Z, Xu G. Metal-organic framework nanosheets: Preparation and applications. Coord Chem Rev, 2019, 388: 79–106
76 Rodenas T, Luz I, Prieto G, *et al.* Metal-organic framework nanosheets in polymer composite materials for gas separation. Nat Mater, 2015, 14: 48–55
77 Li F, Wang P, Huang X, *et al.* Large-scale, bottom-up synthesis of binary metal-organic framework nanosheets for efficient water oxidation. Angew Chem Int Ed, 2019, 58: 7051–7056
78 Hu A, Pang Q, Tang C, *et al.* Epitaxial growth and integration of insulating metal-organic frameworks in electrochemistry. J Am Chem

Soc, 2019, 141: 11322–11327
79 Zhuang L, Ge L, Liu H, *et al.* A surfactant-free and scalable general strategy for synthesizing ultrathin two-dimensional metal-organic framework nanosheets for the oxygen evolution reaction. Angew Chem Int Ed, 2019, 58: 13565–13572
80 Amo-Ochoa P, Welte L, González-Prieto R, *et al.* Single layers of a multifunctional laminar Cu(I,II) coordination polymer. Chem Commun, 2010, 46: 3262–3264
81 Li PZ, Maeda Y, Xu Q. Top-down fabrication of crystalline metal-organic framework nanosheets. Chem Commun, 2011, 47: 8436–8438
82 Foster JA, Henke S, Schneemann A, *et al.* Liquid exfoliation of alkyl-ether functionalised layered metal-organic frameworks to nanosheets. Chem Commun, 2016, 52: 10474–10477
83 Le TH, Oh Y, Kim H, *et al.* Exfoliation of 2D materials for energy and environmental applications. Chem Eur J, 2020, 26: 6360–6401
84 Kondo A, Tiew CC, Moriguchi F, *et al.* Fabrication of metal-organic framework nanosheets and nanorolls with N-donor type bridging ligands. Dalton Trans, 2013, 42: 15267
85 Mishra RS, Bieler TR, Mukherjee AK. Superplasticity in powder metallurgy aluminum alloys and composites. Acta Metall Mater, 1995, 43: 877–891
86 Chakraborty G, Park IH, Medishetty R, *et al.* Two-dimensional metal-organic framework materials: Synthesis, structures, properties and applications. Chem Rev, 2021, 121: 3751–3891
87 Peng Y, Li Y, Ban Y, *et al.* Two-dimensional metal-organic framework nanosheets for membrane-based gas separation. Angew Chem Int Ed, 2017, 56: 9757–9761
88 Wang X, Chi C, Zhang K, *et al.* Reversed thermo-switchable molecular sieving membranes composed of two-dimensional metal-organic nanosheets for gas separation. Nat Commun, 2017, 8: 14460
89 Chi C, Wang X, Peng Y, *et al.* Facile preparation of graphene oxide membranes for gas separation. Chem Mater, 2016, 28: 2921–2927
90 Cliffe MJ, Castillo-Martínez E, Wu Y, *et al.* Metal-organic nanosheets formed *via* defect-mediated transformation of a hafnium metal-organic framework. J Am Chem Soc, 2017, 139: 5397–5404
91 Li Y, Huang J, Mo ZW, *et al.* Multistep evolution from a metal-organic framework to ultrathin nanosheets. Sci Bull, 2019, 64: 964–967
92 Pang W, Shao B, Tan XQ, *et al.* Exfoliation of metal-organic frameworks into efficient single-layer metal-organic nanosheet electrocatalysts by the synergistic action of host-guest interactions and sonication. Nanoscale, 2020, 12: 3623–3629
93 Au VKM, Nakayashiki K, Huang H, *et al.* Stepwise expansion of layered metal-organic frameworks for nonstochastic exfoliation into porous nanosheets. J Am Chem Soc, 2019, 141: 53–57
94 Huang J, Wu JQ, Shao B, *et al.* Ion-induced delamination of layered bulk metal-organic frameworks into ultrathin nanosheets for boosting the oxygen evolution reaction. ACS Sustain Chem Eng, 2020, 8: 10554–10563
95 Li Y, Mo ZW, Zhang XW, *et al.* A metal-ligand layer compatible with various types of pillars for new porous coordination polymers. Cryst Growth Des, 2020, 20: 7021–7026
96 Lu WG, Jiang L, Feng XL, *et al.* Four 3D porous metal-organic frameworks with various layered and pillared motifs. Cryst Growth Des, 2008, 8: 986–994
97 Zhang JH, Yang W, Zhang M, *et al.* Metal-organic layers as a platform for developing single-atom catalysts for photochemical CO_2 reduction. Nano Energy, 2021, 80: 105542
98 Kambe T, Sakamoto R, Kusamoto T, *et al.* Redox control and high conductivity of nickel bis(dithiolene) complex π-nanosheet: A potential organic two-dimensional topological insulator. J Am Chem Soc, 2014, 136: 14357–14360
99 Sakamoto R, Hoshiko K, Liu Q, *et al.* A photofunctional bottom-up bis(dipyrrinato)zinc(II) complex nanosheet. Nat Commun, 2015, 6: 6713
100 Tsukamoto T, Takada K, Sakamoto R, *et al.* Coordination nanosheets based on terpyridine-zinc(II) complexes: As photoactive host materials. J Am Chem Soc, 2017, 139: 5359–5366
101 Clough AJ, Yoo JW, Mecklenburg MH, *et al.* Two-dimensional metal-organic surfaces for efficient hydrogen evolution from water. J Am Chem Soc, 2014, 137: 118–121
102 Clough AJ, Skelton JM, Downes CA, *et al.* Metallic conductivity in a two-dimensional cobalt dithiolene metal-organic framework. J Am Chem Soc, 2017, 139: 10863–10867
103 Bauer T, Zheng Z, Renn A, *et al.* Synthesis of free-standing, monolayered organometallic sheets at the air/water interface. Angew Chem Int Ed, 2011, 50: 7879–7884
104 Dong R, Pfeffermann M, Liang H, *et al.* Large-area, free-standing, two-dimensional supramolecular polymer single-layer sheets for highly efficient electrocatalytic hydrogen evolution. Angew Chem Int Ed, 2015, 54: 12058–12063
105 Dong R, Zheng Z, Tranca DC, *et al.* Immobilizing molecular metal dithiolene-diamine complexes on 2D metal-organic frameworks for electrocatalytic H_2 production. Chem Eur J, 2017, 23: 2255–2260
106 Jiang Y, Ryu GH, Joo SH, *et al.* Porous two-dimensional monolayer metal-organic framework material and its use for the size-selective separation of nanoparticles. ACS Appl Mater Interfaces, 2017, 9: 28107–28116
107 Wang L, Sahabudeen H, Zhang T, *et al.* Liquid-interface-assisted synthesis of covalent-organic and metal-organic two-dimensional crystalline polymers. npj 2D Mater Appl, 2018, 2: 26
108 Sakaida S, Otsubo K, Sakata O, *et al.* Crystalline coordination framework endowed with dynamic gate-opening behaviour by being downsized to a thin film. Nat Chem, 2016, 8: 377–383
109 Chen DM, Zhang NN, Tian JY, *et al.* Pore modulation of metal-organic frameworks towards enhanced hydrothermal stability and acetylene uptake *via* incorporation of different functional brackets. J Mater Chem A, 2017, 5: 4861–4867
110 Wang B, Luo Y, Liu B, *et al.* Field-effect transistor based on an *in situ* grown metal-organic framework film as a liquid-gated sensing device. ACS Appl Mater Interfaces, 2019, 11: 35935–35940
111 Yang C, Schellhammer KS, Ortmann F, *et al.* Coordination polymer framework based on-chip micro-supercapacitors with AC line-filtering performance. Angew Chem Int Ed, 2017, 56: 3920–3924
112 Farha OK, Hupp JT. Rational design, synthesis, purification, and activation of metal-organic framework materials. Acc Chem Res, 2010, 43: 1166–1175
113 Xu G, Yamada T, Otsubo K, *et al.* Facile "modular assembly" for fast construction of a highly oriented crystalline MOF nanofilm. J Am Chem Soc, 2012, 134: 16524–16527
114 Li G, Zhang X, Zhang H, *et al.* Bottom-up MOF-intermediated synthesis of 3D hierarchical flower-like cobalt-based homobimetallic phophide composed of ultrathin nanosheets for highly efficient oxygen evolution reaction. Appl Catal B-Environ, 2019, 249: 147–154
115 Zheng S, Li B, Tang Y, *et al.* Ultrathin nanosheet-assembled $[Ni_3(OH)_2(PTA)_2(H_2O)_4]\cdot 2H_2O$ hierarchical flowers for high-performance electrocatalysis of glucose oxidation reactions. Nanoscale, 2018, 10: 13270–13276
116 Zhong H, Ly KH, Wang M, *et al.* A phthalocyanine-based layered two-dimensional conjugated metal-organic framework as a highly efficient electrocatalyst for the oxygen reduction reaction. Angew Chem Int Ed, 2019, 58: 10677–10682
117 Xu G, Otsubo K, Yamada T, *et al.* Superprotonic conductivity in a highly oriented crystalline metal-organic framework nanofilm. J Am Chem Soc, 2013, 135: 7438–7441
118 Wang Y, Zhao M, Ping J, *et al.* Bioinspired design of ultrathin 2D bimetallic metal-organic-framework nanosheets used as biomimetic enzymes. Adv Mater, 2016, 28: 4149–4155
119 Huang Y, Zhao M, Han S, *et al.* Growth of Au nanoparticles on 2D metalloporphyrinic metal-organic framework nanosheets used as biomimetic catalysts for cascade reactions. Adv Mater, 2017, 29: 1700102
120 Zhao M, Wang Y, Ma Q, *et al.* Ultrathin 2D metal-organic framework nanosheets. Adv Mater, 2015, 27: 7372–7378
121 Cao F, Zhao M, Yu Y, *et al.* Synthesis of two-dimensional $CoS_{1.097}$/nitrogen-doped carbon nanocomposites using metal-organic framework nanosheets as precursors for supercapacitor application. J Am Chem Soc, 2016, 138: 6924–6927
122 Cao L, Lin Z, Peng F, *et al.* Self-supporting metal-organic layers as

single-site solid catalysts. Angew Chem Int Ed, 2016, 55: 4962–4966
123 Shi W, Cao L, Zhang H, *et al.* Surface modification of two-dimensional metal-organic layers creates biomimetic catalytic microenvironments for selective oxidation. Angew Chem Int Ed, 2017, 56: 9704–9709
124 Gedanken A. Using sonochemistry for the fabrication of nanomaterials. Ultrasons Sonochem, 2004, 11: 47–55
125 Xu H, Zeiger BW, Suslick KS. Sonochemical synthesis of nanomaterials. Chem Soc Rev, 2013, 42: 2555–2567
126 Zhao S, Wang Y, Dong J, *et al.* Ultrathin metal-organic framework nanosheets for electrocatalytic oxygen evolution. Nat Energy, 2016, 1: 16184
127 Wang Y, Liu Y, Wang H, *et al.* Ultrathin NiCo-MOF nanosheets for high-performance supercapacitor electrodes. ACS Appl Energy Mater, 2019, 2: 2063–2071
128 Hai G, Jia X, Zhang K, *et al.* High-performance oxygen evolution catalyst using two-dimensional ultrathin metal-organic frameworks nanosheets. Nano Energy, 2018, 44: 345–352
129 Ning Y, Lou X, Li C, *et al.* Ultrathin cobalt-based metal-organic framework nanosheets with both metal and ligand redox activities for superior lithium storage. Chem Eur J, 2017, 23: 15984–15990
130 Zhu D, Guo C, Liu J, *et al.* Two-dimensional metal-organic frameworks with high oxidation states for efficient electrocatalytic urea oxidation. Chem Commun, 2017, 53: 10906–10909
131 Cai M, Liu Q, Xue Z, *et al.* Constructing 2D MOFs from 2D LDHs: A highly efficient and durable electrocatalyst for water oxidation. J Mater Chem A, 2020, 8: 190–195
132 Chen J, Zhuang P, Ge Y, *et al.* Sublimation-vapor phase pseudomorphic transformation of template-directed MOFs for efficient oxygen evolution reaction. Adv Funct Mater, 2019, 29: 1903875
133 Sun F, Wang G, Ding Y, *et al.* NiFe-based metal-organic framework nanosheets directly supported on nickel foam acting as robust electrodes for electrochemical oxygen evolution reaction. Adv Energy Mater, 2018, 8: 1800584
134 Yang L, Zhu G, Wen H, *et al.* Constructing a highly oriented layered MOF nanoarray from a layered double hydroxide for efficient and long-lasting alkaline water oxidation electrocatalysis. J Mater Chem A, 2019, 7: 8771–8776
135 Deng T, Lu Y, Zhang W, *et al.* Inverted design for high-performance supercapacitor *via* $Co(OH)_2$-derived highly oriented MOF electrodes. Adv Energy Mater, 2018, 8: 1702294
136 Zhuang L, Ge L, Yang Y, *et al.* Ultrathin iron-cobalt oxide nanosheets with abundant oxygen vacancies for the oxygen evolution reaction. Adv Mater, 2017, 29: 1606793
137 Yuan S, Feng L, Wang K, *et al.* Stable metal-organic frameworks: Design, synthesis, and applications. Adv Mater, 2018, 30: 1704303
138 Cho W, Lee HJ, Oh M. Growth-controlled formation of porous coordination polymer particles. J Am Chem Soc, 2008, 130: 16943–16946
139 Sakata Y, Furukawa S, Kondo M, *et al.* Shape-memory nanopores induced in coordination frameworks by crystal downsizing. Science, 2013, 339: 193–196
140 He S, Chen Y, Zhang Z, *et al.* Competitive coordination strategy for the synthesis of hierarchical-pore metal-organic framework nanostructures. Chem Sci, 2016, 7: 7101–7105
141 Pham MH, Vuong GT, Fontaine FG, *et al.* Rational synthesis of metal-organic framework nanocubes and nanosheets using selective modulators and their morphology-dependent gas-sorption properties. Cryst Growth Des, 2012, 12: 3091–3095
142 Schaate A, Roy P, Godt A, *et al.* Modulated synthesis of Zr-based metal-organic frameworks: From nano to single crystals. Chem Eur J, 2011, 17: 6643–6651
143 Tsuruoka T, Furukawa S, Takashima Y, *et al.* Nanoporous nanorods fabricated by coordination modulation and oriented attachment growth. Angew Chem Int Ed, 2009, 48: 4739–4743
144 Nian P, Liu H, Zhang X. Bottom-up synthesis of 2D Co-based metal-organic framework nanosheets by an ammonia-assisted strategy for tuning the crystal morphology. CrystEngComm, 2019, 21: 3199–3208
145 Seoane B, Coronas J, Gascon I, *et al.* Metal-organic framework based mixed matrix membranes: A solution for highly efficient CO_2 capture? Chem Soc Rev, 2015, 44: 2421–2454
146 Zheng Z, Grünker R, Feng X. Synthetic two-dimensional materials: A new paradigm of membranes for ultimate separation. Adv Mater, 2016, 28: 6529–6545
147 Cheng Y, Wang X, Jia C, *et al.* Ultrathin mixed matrix membranes containing two-dimensional metal-organic framework nanosheets for efficient CO_2/CH_4 separation. J Membrane Sci, 2017, 539: 213–223
148 Kang Z, Peng Y, Hu Z, *et al.* Mixed matrix membranes composed of two-dimensional metal-organic framework nanosheets for pre-combustion CO_2 capture: A relationship study of filler morphology *versus* membrane performance. J Mater Chem A, 2015, 3: 20801–20810
149 Xue F, Kumar P, Xu W, *et al.* Direct synthesis of 7 nm-thick zinc(II)-benzimidazole-acetate metal-organic framework nanosheets. Chem Mater, 2017, 30: 69–73
150 Yang Y, Goh K, Wang R, *et al.* High-performance nanocomposite membranes realized by efficient molecular sieving with CuBDC nanosheets. Chem Commun, 2017, 53: 4254–4257
151 He T, Ni B, Zhang S, *et al.* Ultrathin 2D zirconium metal-organic framework nanosheets: Preparation and application in photocatalysis. Small, 2018, 14: 1703929
152 Hu Z, Mahdi EM, Peng Y, *et al.* Kinetically controlled synthesis of two-dimensional Zr/Hf metal-organic framework nanosheets *via* a modulated hydrothermal approach. J Mater Chem A, 2017, 5: 8954–8963
153 Lin Z, Thacker NC, Sawano T, *et al.* Metal-organic layers stabilize earth-abundant metal-terpyridine diradical complexes for catalytic C–H activation. Chem Sci, 2018, 9: 143–151
154 Yu Y, Wu XJ, Zhao M, *et al.* Anodized aluminum oxide templated synthesis of metal-organic frameworks used as membrane reactors. Angew Chem Int Ed, 2017, 56: 578–581
155 Zhang S, Ye H, Hua J, *et al.* Recent advances in dye-sensitized photoelectrochemical cells for water splitting. EnergyChem, 2019, 1: 100015
156 Liu D, Ouyang T, Xiao R, *et al.* Anchoring Co^{II} ions into a thiol-laced metal-organic framework for efficient visible-light-driven conversion of CO_2 into CO. ChemSusChem, 2019, 12: 2166–2170
157 Cao LM, Lu D, Zhong DC, *et al.* Prussian blue analogues and their derived nanomaterials for electrocatalytic water splitting. Coord Chem Rev, 2020, 407: 213156
158 Liu DC, Zhong DC, Lu TB. Non-noble metal-based molecular complexes for CO_2 reduction: From the ligand design perspective. EnergyChem, 2020, 2: 100034
159 Gong YN, Shao BZ, Mei JH, *et al.* Facile synthesis of C_3N_4-supported metal catalysts for efficient CO_2 photoreduction. Nano Res, 2022, 15: 551–556
160 Wang J, Feng YX, Zhang M, *et al.* β-Cyclodextrin decorated CdS nanocrystals boosting the photocatalytic conversion of alcohols. CCS Chem, 2020, 2: 81–88
161 Zhang J, Zhong D, Lu T. Co(II)-based molecular complexes for photochemical CO_2 reduction. Acta Physico Chim Sin, 2020, 0: 2008068–0
162 Deng JH, Luo J, Mao YL, *et al.* π–π stacking interactions: Non-negligible forces for stabilizing porous supramolecular frameworks. Sci Adv, 2020, 6: eaax9976
163 Liang Z, Zhao R, Qiu T, *et al.* Metal-organic framework-derived materials for electrochemical energy applications. EnergyChem, 2019, 1: 100001
164 Li X, Zhu QL. MOF-based materials for photo- and electrocatalytic CO_2 reduction. EnergyChem, 2020, 2: 100033
165 Li Y, Jia B, Chen B, *et al.* MOF-derived Mn doped porous CoP nanosheets as efficient and stable bifunctional electrocatalysts for water splitting. Dalton Trans, 2018, 47: 14679–14685
166 Li FL, Shao Q, Huang X, *et al.* Nanoscale trimetallic metal-organic frameworks enable efficient oxygen evolution electrocatalysis. Angew Chem Int Ed, 2018, 57: 1888–1892
167 Wang J, Gan L, Zhang W, *et al. In situ* formation of molecular Ni–Fe active sites on heteroatom-doped graphene as a heterogeneous electrocatalyst toward oxygen evolution. Sci Adv, 2018, 4: eaap7970
168 Lu XF, Liao PQ, Wang JW, *et al.* An alkaline-stable, metal hydroxide

mimicking metal-organic framework for efficient electrocatalytic oxygen evolution. J Am Chem Soc, 2016, 138: 8336–8339
169 Xiao X, Zhang G, Xu Y, *et al.* A new strategy for the controllable growth of MOF@PBA architectures. J Mater Chem A, 2019, 7: 17266–17271
170 Huang X, Zhang Y, Shen H, *et al.* N-doped carbon nanosheet networks with favorable active sites triggered by metal nanoparticles as bifunctional oxygen electrocatalysts. ACS Energy Lett, 2018, 3: 2914–2920
171 Nai J, Lu Y, Yu L, *et al.* Formation of Ni–Fe mixed diselenide nanocages as a superior oxygen evolution electrocatalyst. Adv Mater, 2017, 29: 1703870
172 Hod I, Sampson MD, Deria P, *et al.* Fe-porphyrin-based metal-organic framework films as high-surface concentration, heterogeneous catalysts for electrochemical reduction of CO_2. ACS Catal, 2015, 5: 6302–6309
173 Ye L, Liu J, Gao Y, *et al.* Highly oriented MOF thin film-based electrocatalytic device for the reduction of CO_2 to CO exhibiting high faradaic efficiency. J Mater Chem A, 2016, 4: 15320–15326
174 Wu JX, Yuan WW, Xu M, *et al.* Ultrathin 2D nickel zeolitic imidazolate framework nanosheets for electrocatalytic reduction of CO_2. Chem Commun, 2019, 55: 11634–11637
175 Zhu W, Zhang C, Li Q, *et al.* Selective reduction of CO_2 by conductive MOF nanosheets as an efficient co-catalyst under visible light illumination. Appl Catal B-Environ, 2018, 238: 339–345
176 Ren JT, Zheng YL, Yuan K, *et al.* Self-templated synthesis of Co_3O_4 hierarchical nanosheets from a metal-organic framework for efficient visible-light photocatalytic CO_2 reduction. Nanoscale, 2020, 12: 755–762
177 Kreno LE, Leong K, Farha OK, *et al.* Metal-organic framework materials as chemical sensors. Chem Rev, 2012, 112: 1105–1125
178 Xu H, Gao J, Qian X, *et al.* Metal-organic framework nanosheets for fast-response and highly sensitive luminescent sensing of Fe^{3+}. J Mater Chem A, 2016, 4: 10900–10905
179 Ning D, Liu Q, Wang Q, *et al.* Luminescent MOF nanosheets for enzyme assisted detection of H_2O_2 and glucose and activity assay of glucose oxidase. Sens Actuat B-Chem, 2019, 282: 443–448
180 He C, Lu K, Lin W. Nanoscale metal-organic frameworks for real-time intracellular pH sensing in live cells. J Am Chem Soc, 2014, 136: 12253–12256
181 Zhao Y, Jiang L, Shangguan L, *et al.* Synthesis of porphyrin-based two-dimensional metal-organic framework nanodisk with small size and few layers. J Mater Chem A, 2018, 6: 2828–2833
182 Hai X, Li N, Wang K, *et al.* A fluorescence aptasensor based on two-dimensional sheet metal-organic frameworks for monitoring adenosine triphosphate. Anal Chim Acta, 2018, 998: 60–66
183 He L, Duan F, Song Y, *et al.* 2D zirconium-based metal-organic framework nanosheets for highly sensitive detection of mucin 1: Consistency between electrochemical and surface plasmon resonance methods. 2D Mater, 2017, 4: 025098
184 Lu W, Wu X. Ni-MOF nanosheet arrays: Efficient non-noble-metal electrocatalysts for non-enzymatic monosaccharide sensing. New J Chem, 2018, 42: 3180–3183
185 Song WJ. Intracellular DNA and microRNA sensing based on metal-organic framework nanosheets with enzyme-free signal amplification. Talanta, 2017, 170: 74–80

Acknowledgements This work was financially supported by the National Key R&D Program of China (2017YFA0700104), the National Natural Science Foundation of China (22071182, 21861001, 21931007 and 21790052), the 111 Project of China (D17003), and the Science & Technology Development Fund of Tianjin Education Commission for Higher Education (2018KJ129).

Author contributions Wang H investigated the relevant literature and wrote this manuscript. Zhong D and Lu T carefully reviewed and modified this manuscript. Zhang C and Dong B gave some valuable suggestions on revision. All authors contributed to the general discussion.

Conflict of interest The authors declare that they have no conflict of interest.

Huifeng Wang received her ME degree in 2020 from Guangxi Normal University. Currently, she is pursuing her PhD degree at Yangzhou University. Her research focuses on the rational design and synthesis of functional complexes for energy storage and conversion.

Dichang Zhong obtained his BS degree in 2003 from Gannan Normal University, MS degree in 2006 from Guangxi Normal University, and PhD degree in 2011 from Sun Yat-Sen University. Then, he joined the faculty at Gannan Normal University. He worked as a Japan Society for the Promotion of Science (JSPS) postdoctoral fellow at the National Institute of Advanced Industrial Science and Technology (AIST), Japan, for two years. In 2020, he moved to Tianjin University of Technology. His interests focus on the design and synthesis of molecular catalytic materials for energy storage and conversion.

Tongbu Lu obtained his BS degree in 1988 and his PhD degree in 1993 from Lanzhou University. After two years of a postdoctoral fellowship at Sun Yat-Sen University, he joined the faculty at the same university and became a professor in 2000. He worked as a postdoctoral fellow in F. Albert Cotton's group at Texas A&M University in 1998 and 2002. In 2016, he moved to Tianjin University of Technology. His research interests focus on the study of artificial photosynthesis, including the design of homogeneous and heterogeneous catalysts for water splitting and CO_2 reduction.

金属有机层: 制备与应用

王慧锋[1,2], 张超[1], 董宝霞[2], 钟地长[1*], 鲁统部[1*]

摘要 金属有机层(MOLs)以其独特的特性在材料科学中引起了广泛的关注. 近十年来, MOLs在合成和应用方面发展迅速. 本文综述了MOLs的最新研究进展. 首先, 我们介绍了MOLs的两种制备方法, 即自上而下和自下而上的方法. 然后, 我们讨论了MOLs在气体分离、催化、能源催化和转化以及化学传感器等方面的应用, 重点揭示了MOLs的性能-形貌/结构关系. 最后, 我们展望了MOLs在未来发展的机遇和挑战.

